The performance of BM@N spectrometer

BMN collaboration

February 2023

1 Introduction

BM@N (baryonic matter at Nuclotron) is the first experiment operational at the ion-accelerating complex Nuclotron/NICA, studying interactions of relativistic ion beams of heavy ions with fixed targets [1] in the energy range of high densities of baryonic matter [2]. At the Nuclotron energies, the density of nucleons in a fireball created by two colliding heavy nuclei is 3-4 times higher than the nuclear saturation density[3]. In addition, these energies are high enough to study strange mesons and (multi)-strange hyperons produced in nucleus-nucleus collisions close to the kinematic threshold [4, 5]. The primary goal of the experiment is to constrain parameters of the equation of state (EoS) of high-density nuclear matter. Studies of the excitation function of strange particle production below and near to the kinematical threshold make it possible to distinguish hard behaviour of the EoS from the soft one [6].

The Nuclotron will provide the experiment with beams of a variety of particles, from protons to gold ions, with kinetic energy in the range from 1 to 6 GeV/nucleon for light ions with Z/A ratio of ~ 0.5 and up to 4.5 GeV/nucleon for heavy ions with Z/A ratio of ~ 0.4.

The BM@N detector is a forward spectrometer covering the pseudorapidity range $1.6 \leq \eta \leq 4.4$. Schematic view of the BM@N setup is shown in Fig. 1. The description of the spectrometer subsystems is organised in a "downstream beam" order. The details for all subsystems are given in a corresponding sections below.

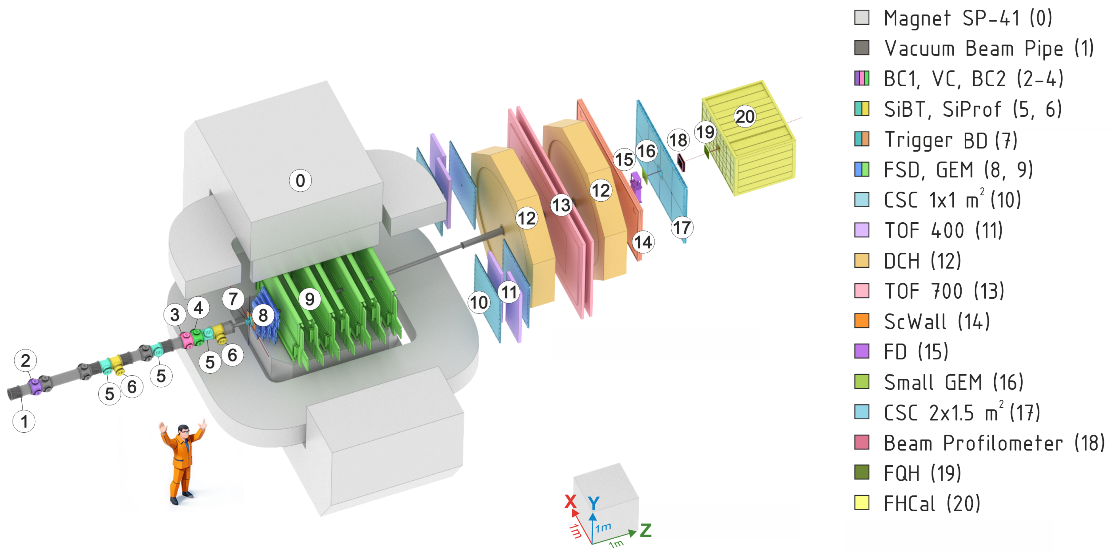

Figure 1: Schematic view of BM@N setup in RUN8.

2 Beamline

2.1 Beam transport

The BM@N experiment is part of the NICA complex (see Fig. 2), located on the extracted beam from the Nuclotron in the target hall.

Electronic string source of the highly-charged ions "KRION-6", provides heavy ions of Au^{31+} (up to $2 * 10^9$ per pulse with a pulse repetition rate of 10 Hz) and delivers them into the HILac.

The main tasks of the booster are as follows:

• accumulation of ions at an injection energy of $2.5 * 10^9$ $^{197}Au^{31+}$ ions;

• effective acceleration of incompletely stripped ions, which is possible due to the ultrahigh vacuum in the beam chamber;

• formation of the required phase volume of the beam using an ECS at an energy of 65 MeV/n;

• acceleration of heavy ions to the energy required for their efficient stripping;

• fast (single-lap) extraction of the accelerated beam for its injection into the Nuclotron.

The Nuclotron SC proton synchrotron has three operation modes:

• Acceleration of heavy ions for storage in the collider.

• Acceleration of polarized protons and deuterons for feeding the collider.

• Acceleration of both polarized and unpolarized protons and deuterons and heavy ions for internal target experiments or slow extraction to fixed target experiments.

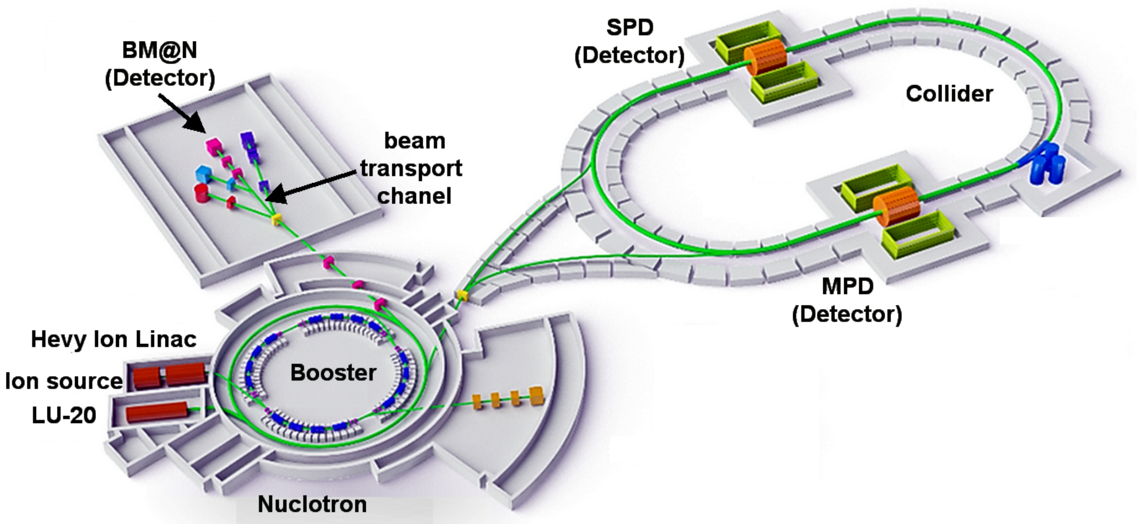

Figure 2: Complex NICA.

The beam extracted from the Nuclotron is transported to the BM@N experimental area over a distance of about 110 m by a set of dipole magnets and quadrupole lenses. At the entrance of the BM@N setup the position and direction of the beam are already close to those required to bring the beam to the target, and only relatively small adjustments are needed in order to provide final steering of the beam. These corrections are performed by a pair of dipole magnets, VKM and SP-57, which allow bending in vertical and horizontal planes and have maximum current 250A and 600A respectively. The centers of these magnets are positioned at approximately 7.7 and 5.7 m from the target (Fig. 3). In addition, a doublet of quadrupole lenses, 1k200 and 2k200, each having the maximum current of 2500A, allows optimal focusing of the beam on the target. The corresponding position of their centers is at about 12.5 and 10.0 m upstream of the target.

The target is located inside the analyzing magnet SP-41, therefore, after passing through the target, the beam ions are deflected by the magnetic field of SP-41 (maximum current 2000A, Bdl = xxx Tm). It should be noted that for experiments with heavy ions it is essential to enclose the beam transport channel in vacuum, including the part that goes through the analysing magnet. This requirement combined with precise placement of the tracking detectors inside the SP-41 does not allow quick reconfiguration of the detectors for different beam momenta, making it necessary to adjust the magnetic field of the analysing magnet depending on the choice of the beam momentum. Studies of the Xe + CsI collisions during the 2022-2023 run were performed at beam energies of 3.0 GeV/n and 3.8 GeV/n, and the current of the SP-41 was set to 1395 and 1720 A respectively.

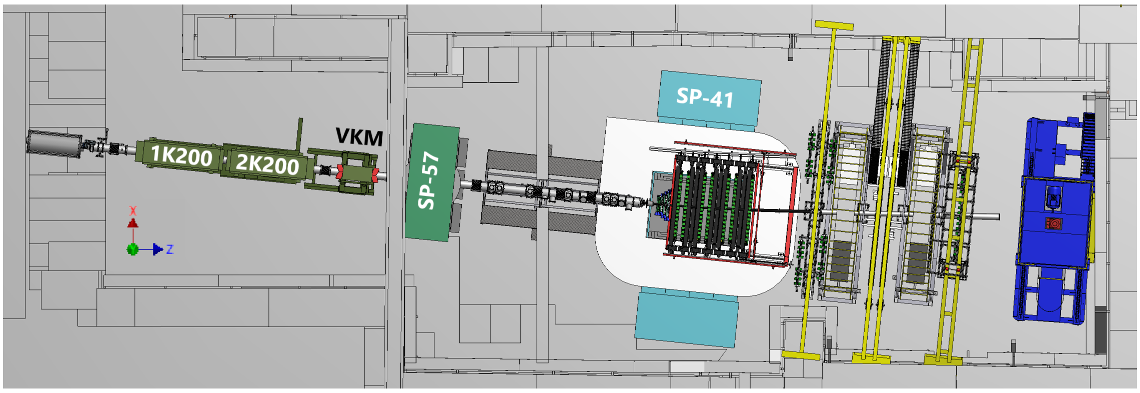

Figure 3: Magnetic elements of the BM@N setup.

2.2 Vacuum beam pipe

A vacuum beam pipe was integrated into the experimental setup in order to minimize the amount of scattering material on the way of heavy ion beam. The beam pipe has continuous vacuum, but in terms of components and material of the tube it can be subdivided into four large parts: the first section covers the region upstream of the magnet SP-57 and within the magnet itself, the second section goes up to the target, the third section is placed inside the analyzing magnet SP-41 and the last section is located after the analyzing magnet. Vacuum in the entire beam pipe at the BM@N setup is achieved by a single roots pump installed upstream of the 1K200 quadrupole lense. The pressure maintained during the experiment is at the level of 10^{-4} Torr. With the exception of the third part, the configuration of vacuum pipe and its components were designed, manufactured and tested by LLC Vacuum systems and technologies (Belgorod, Russia). ISO-K vacuum standard is accepted for flange connections, however, significant fraction of the components was custom made in order to meet limitations posed by aperture of the magnets and geometry of the detectors.

The first part of the beam pipe is designed to create vacuum in the area of beam transport through 1K200 and 2K200 quadrupole lenses and through corrective magnets VKM and SP-57. This part of the vacuum pipe is made of stainless steel, has length of 11.7 m and outer diameter 200mm. Two slide gates are installed in this section, one in the front of the 1K200 lense and another after the VKM magnet. The vacuum level is monitored by two vacuum gauges, the data from which are recorded in the slow control system.

The second part of the beam pipe serves to create vacuum in the region between the SP-57 magnet and the target node located inside the SP-41 magnet. This part of the beam pipe is xxx m long and also has outer diameter 200mm. It includes vacuum boxes containing beam detectors described in the next section: two 3-way boxes for profilometers, three 3-way boxes for silicon tracker and three 6-way boxes for trigger counters BC1, BC2 and VC. All boxes located outside the magnetic field of the analyzing magnet SP-41 are made of stainless steel, while the vacuum pipe components, which have to be close to the target and therefore placed in the magnet, are made of aluminum: compensator and three boxes for profilometer, Si beam tracker and BC2. Bending of the beam ion trajectories by the magnetic field leads to a deflection from a straight line resulting in a few mm displacement in X direction at the target location. During the assembly of vacuum elements of the beam pipe, an adjustment is carried out in order to compensate for this deflection. For that purpose the corresponding groves for O-rings of the vacuum boxes are made slightly wider than dictated by the ISO standard and allow slight off-center shifts of the vacuum pipe components. The target flange assembly is also made of aluminum as well as an ISO240 to 66 mm vacuum adapter for connection with the vacuum tube of the third section.

The third part of the beam pipe is 4.5 m long and made of carbon fiber by so-and-so producer. The entire carbon pipe consists of four straight segments of different lengths connected to each other by flangeless carbon fiber connections, which provide possibility to align sections at slight angles with respect to each other as shown in Fig. 4 and 5. The rotation angles were evaluated by the simulation of the 4.5 AGeV (???) gold ions trajectories in the magnetic field of SP-41 at current xxx A. The carbon beam pipe is suspended on two supports also made of carbon fiber and installed on two lower GEM detectors, the one closest to the target and the most downstream. The supports have adjustment units for precise positioning of the carbon beam pipe on the beam axis (Fig. 5). The carbon beam pipe was designed to sustain vacuum up to 10^{-4} Torr. In the straight segments the thickness is about 1 mm, while in flangeless connections it reaches 2 mm.

The fourth part of the beam pipe provides vacuum volume along the beam trajectory through

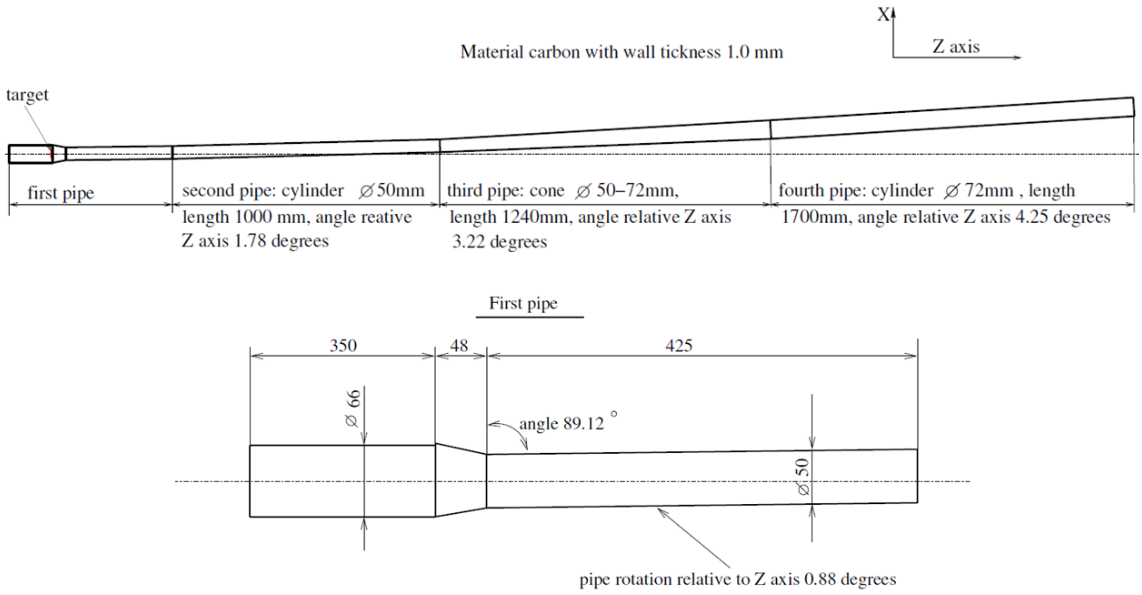

Figure 4: Technical design of the carbon beam pipe.

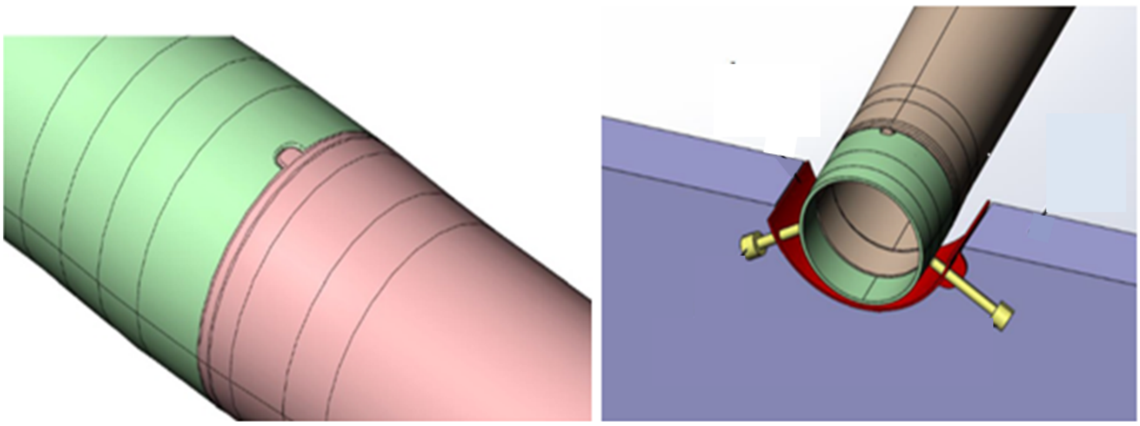

Figure 5: 3D models of the dismountable flangeless connection (left) and the support scheme of the carbon beam pipe in the GEM beam hole (right).

the outer tracker system. The pipes and flanges of this section as well as connection to the carbon beam pipe are made from aluminum (Fig. 6). It has overall length of about 3.2 m (?) and consists of three straight segments 1.2, 0.96 and 1.0 meter long, made from tube with outer diameter of 125 mm and wall thickness of xx mm. At the end of this section, the overall vacuum line is closed by a 100 μm thick titanium membrane installed in ... (?) after the adapter for a diameter of 150 mm.

2.3 Target station

The target station is located at the end of the second beam pipe section. It is designed to provide a possibility to insert a target in the beam line inside the vacuum volume and to interchange several targets without breaking the vacuum. The model and photo of the target station are presented in (Fig. 7). An aluminum flange of 240 mm in diameter serves as a holder of the target assembly elements and as an adapter between the beam pipe upstream of the target station and the first section of the carbon beam pipe. On the outer part of this flange, four pneumatic cylinders are installed providing capability to move in and out of the beam four target frames interchangeably. The pneumatic cylinders are produced by FESTO and allow remote operation. An optocoupler sensor is used in order to control the target position via a special electronic module.

The part of the target assembly placed inside the vacuum can be divided into three components:

1) Centering frame, which fits into the inner part of the first section of the carbon beam pipe.

2) Four petals, in which the targets themselves are installed. In the normal state, all petals are leaning against the side surface of the beam pipe.

Figure 6: Carbon beam pipe connected by a flange to aluminum beam pipe in the BM@N setup.

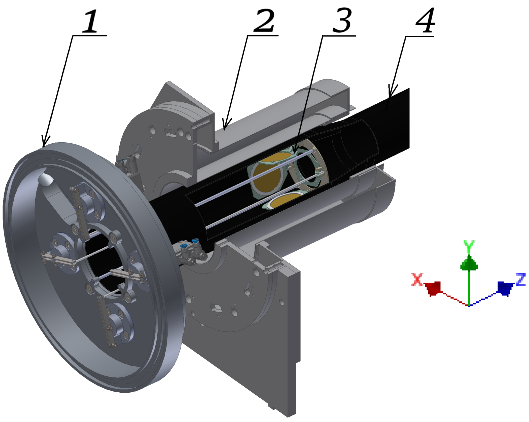

Figure 7: 3D model of target station. 1. Aluminum flange target station. 2. Barrel detector. 3. four targets. 4. Carbon beam pipe.

3) Carbon fiber retaining pins, 300mm long and 3mm in diameter.

In the run with the Xe beam, three disk targets about 3.2 cm in diameter were used: CsI 1.75mm thick, CsI 0.85 mm thick, and Ge 1.02mm thick. One frame of the target assembly was left empty and was used to evaluate the background level caused the particles interactions with the structural elements of the target station.

2.4 Magnetic field of the analysing magnet

The dipole magnet SP-41 with large acceptance is used in the spectrometer as analysing magnet for measurement of momenta of produced particles and beam fragments. In the course of preparation of the magnet for the BM@N experiment, significant upgrade was done in 2012-2013 from SP-41 initial configuration used in the experiments with a streamer chamber. In particular, the hole for a photocamera in the upper pole was filled with steel in order to improve the uniformity of the magnetic field, and the distance between the poles was increased by about 30 cm in order to provide space required by the GEM chambers of the BM@N. The dimensions of the SP-41 pole in the horizontal direction and in the direction along the beam is about 1.4 and 2.5 m, respectively, while the vertical distance between the upper and lower poles after the upgrade is 1.06 m (Fig. 8). In the BM@N setup the magnet is roughly centered on the beam line, in the horizontal plane the beam axis goes through the magnet close to the center of the poles, while vertically the beam axis is shifted closer to the lower pole by about 40 mm. The leading edge of the pole defines the origin of the z axis, and, correspondingly, the target is installed inside the SP-41 magnet at this position along the beam. The target station is described in more detail in the chapter Targets.

Determination of the momentum of the produced particles requires detailed knowledge of the value and orientation of the magnetic field of the analysing magnet. After the upgrade of the SP-41, the measurement of its field was performed by means of planar and 3D Hall probes [7]. In addition, the shape of the field was calculated by the TOSCA code using known configuration of the yoke and coils material. Prior to the run with Xe beam, in Spring 2022, the measurement of the magnetic field was repeated with a goal to obtain the field map for a wider X,Y,Z range and with smaller steps. The measurements with 3D Hall probes covered (-156, +145 cm), (-38, +54 cm), (-162, +439 cm) and were performed in (126 x 47 x 241) points in X, Y, Z coordinates respectively, allowing one to construct the field map on a $2.4 \times 2.0 \times 2.5$ cm^3 three-dimensional grid (Fig. 8). During simulation and event reconstruction, the magnetic field components in a particular (x,y,z) point are calculated by linear interpolation over eight neighboring measured nodes.

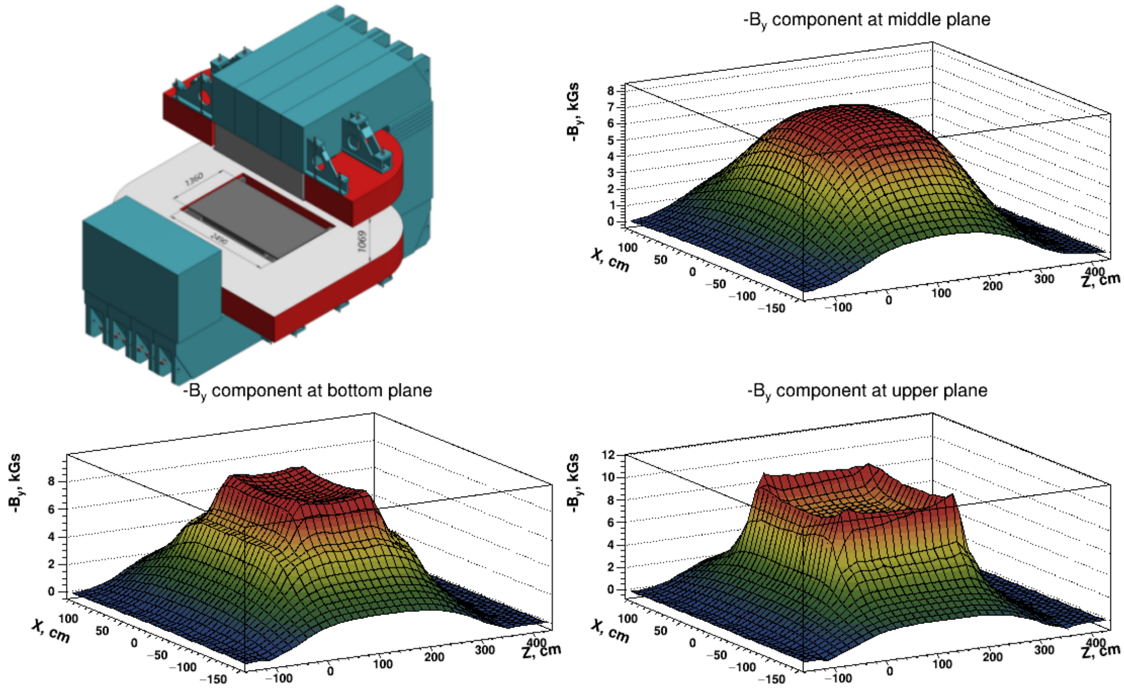

Figure 8: Magnetic field map of the analyzing magnet SP-41.

The measurements of the field map was performed for four values of the current: 900, 1300, 1600, and 1900 A.

3 Beam and trigger detectors

Fig. 9 shows a schematic layout of the trigger detectors, placed on the beam line. In the target area the multiplicity detectors are also shown as a part of the trigger system.

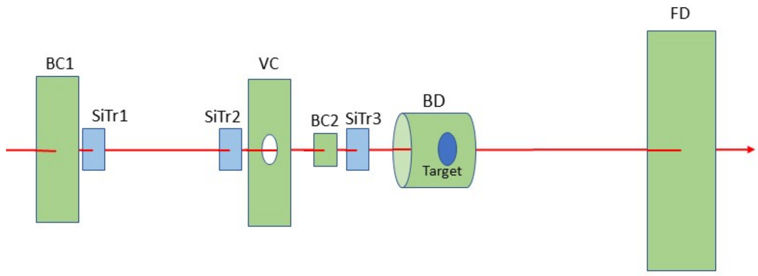

Figure 9: Trigger detectors layout.

Some physical parameters of the beam line detectors are summarized in Table 1.

Aperture of the beam is limited by the 25 mm diameter hole in the scintillation Veto Conter (VC), which rejects the beam halo. The hole diameter in VC is chosen to be large enough to accept most of the beam ions, but smaller than the diameter of the target XX mm. Typically, in the 2023 Xe run, 80% of the beam was accepted by the VC. In order to minimize interactions upstream of the target, scintillators and active parts of silicon detectors are located in vacuum, while the photomultiplier tubes of the scintillation counters and the front-end electronics of the silicon detectors are kept in the air with their housings mounted to the flanges of the beam pipe.

Detector	Z position, cm	Active area, mm x mm	Material	Thickness, mm
BC1	-zz	100 x 100	Scint. BC400B	0.25
BC2	-zz	34 x 34	Scint. BC400B	0.15
VC	-zz	113 x 113 (hole 25)	Plastic	4
SiBTr1	-283	61 x 61	Silicon	0.175
SiBTr2	-183	61 x 61	Silicon	0.175
SiBTr3	-84	61 x 61	Silicon	0.175
FD	+784	150 x 150	Scint. BC408	0.5
Small GEM	+793	100 x 100		
FQH	+970	160 x 160	Quartz	4

Table 1: Parameters of beam and fragment detectors.

In all the beam scintillation counters - BC1, BC2 and VC - light from the scintillator is collected by Al-mylar light guides to a pair of photo-multiplier tubes, placed above and bellow the scintillator. Such orientation of PMT's in BC2 and VC detectors is dictated by the requirement that they should operate in the magnetic field of the analysing magnet, because these counters are located close to the target. Mesh dynode photomultiplier tubes Hamamatsu R2490-07 are used in the detectors BC1 and VC, whereas the BC2 has microchannel plate PMT's Photonis XPM85112/A1 Q400. In addition to beam geometry, the detectors BC1 and BC2 define start time for the time-of-flight system. The requirement to obtain precise time measurement favored the design of BC1 and BC2 with light collection by two PMT's. Both types of photo-multiplier tubes used in these counters have excellent timing characteristics. The signal from each PMT is sent to a fast fan-out module which has time jitter of about 10 ps and preserves high quality of time response. The signal from one output of the fan-out is sent to a TQDC which allows to determine time and amplitude of the pulse. After correction for time walk (slewing), the resolution obtained in 2022 Xe run using the signals from both photo-tubes was found to be 40 ps for BC1 and BC2 individually, and 30 ps for the combined response of the system of two counters. The input in the trigger logic is configured to accept one signal from each of the beam counters, BC1, BC2 and VC. Individual signals from top or bottom PMT's are affected by light collection non-uniformity to a larger degree than a combined signal from two photo-tubes. Therefore, in all counters the signals from top and bottom PMT's are balanced in gain by high-voltage settings, and the signals from the second output of the fan-outs are sent to a passive linear fan-in after which the summed signals are fed to the trigger logic unit. In addition, the summed signals are read-out using TQDC for trigger setting up and monitoring.

Upstream the target the beam position is traced by a set of silicon tracker detectors. The beam tracker system consists of three double-sided silicon strip detectors identical in design. Each detector has 60 mm by 60 mm active area with orthogonal orientation of p+ and n+ strips on two sides. These detectors are kept permanently in the beam and provide information about beam ion trajectory for each event. More detailed description of the beam tracker is given in the next chapter. In addition to the beam tracker, the beam position and profile can also be measured by a pair of beam profilometers which are similar in design and parameters to the beam tracker stations, but have a much courser pitch 1.8 mm in X and Y. The read-out of the profilometers is organised independently of the main BM@N DAQ in order to facilitate beam tuning at the early stages of the run. The detectors of the beam profilometers can be moved in and out of the beam by remotely controlled drivers without breaking the vacuum. During the data accumulation the detectors of the beam profilometers are positioned outside of the beamline.

Trigger detectors sensitive to the multiplicity of particles produced in the interaction include Barrel detector (BD) and Silicon multiplicity detector (SiMD). These detectors, schematically shown in Fig. 10, are placed close to the target in order to cover sufficiently large solid angle for produced particles. The target is situated inside the BD.

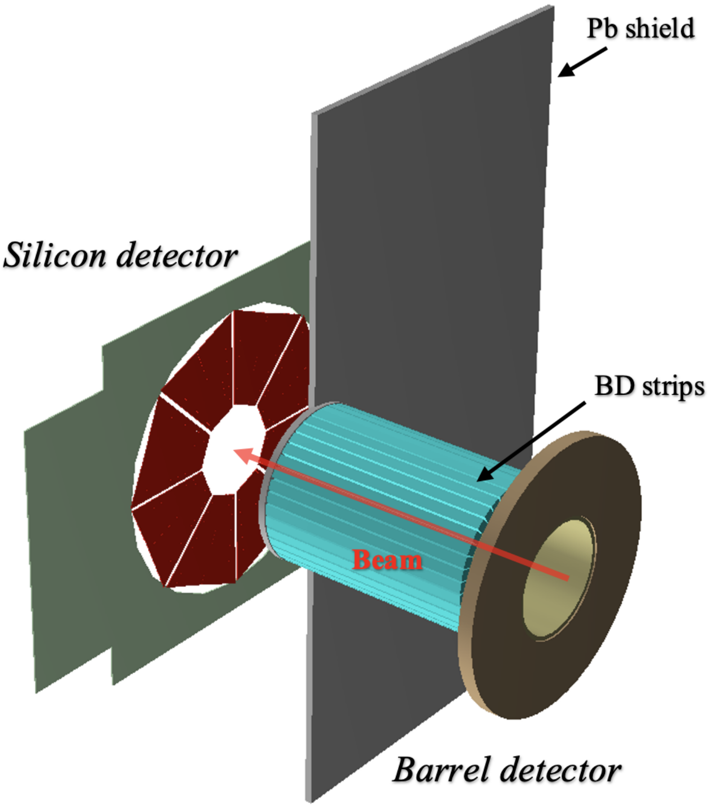

Figure 10: Schematic layout of trigger multiplicity detectors.

The Barrel detector is formed by 40 scintillator strips aligned along the beam line and covering cylindrical surface 90mm in diameter and 150mm long. Each strip of $150 \times 7 \times 7\,mm^3$ size is coated with aluminized mylar and viewed from one side by a silicon photo-multiplier of $6 \times 6\,mm^2$ size (SensL, J-ser.).

Downstream the analysing magnet the beam goes through the Fragment Detector (FD), Small GEM chamber and the Forward quartz hodoscope (FQH). These detectors are placed in the air, the FD is positioned right after the titanium membrane which closes the vacuum pipe line. The amplitude of the pulse in the FD reflects the charge of the ion passing through the counter. This amplitude is used in the trigger system in order to distinguish events with and without interactions in the target. To minimize the background from the interaction within the FD itself, its radiator has to be thin, while in the X and Y directions the radiator should be wide enough to cover all the beam ions going through the target without interaction. The radiator material can be chosen either from scintillator or quartz in experiments with relatively light (up to Xe) or heavy (Au, Bi) beams respectively. For most of data accumulation in the Xe 2022 run the scintillator radiator was used, while the quartz radiator was also evaluated in the short period of the run. The radiator was viewed by a single photo-multiplier tube placed about 50 cm below the beam line. Light collection is done by an air light guide made of aluminized mylar. Pulse height resolution of the FD with the scintillator radiator was found to be 5% for Xe peak.

In addition to the FD the charge of spectator fragment can be determined by the 4mm thick quartz hodoscope FHQ, located in front of the beam hole in the FHCal. Information from this hodoscope is used in the offline analysis for event selection and determination of event centrality. FHQ amplitude resolution for Xe ions is about 2%. The detailed description of the hodoscope is given in the section "Forward Spectator Detectors".

The Small GEM detector is positioned between the FD and FHQ and used to monitor the position, shape and spot size of the beam downstream the analysing magnet. The detector has three GEM foils. Its active area covers 10 cm$\times$10 cm in X and Y, with 256 strips in each coordinate oriented perpendicular to each other.

4 Silicon Beam Tracker

As already mentioned in the previous section, the main task of the Silicon Beam Tracker (SiBT) is to measure the beam ion trajectory in each event and determine primary vertex coordinates and impact angle of the beam projectile. The tracker consists of three stations each of which utilizes a double-sided silicon strip detector (DSSD) with dimensions $(63 \times 63 \times 0.175) mm^3$. DSSD planes are cut from high-resistance mono-crystalline silicon obtained by the Float Zone method. The thickness 175 μm was chosen as the minimum possible, taking into account the limitations of the planar technology applied to 4" (100 mm) wafers. The minimum thickness of the planes allows not only to reduce the amount of material in the beam, but also to decrease the volume of space charge region of the detector and thus to lower the noise caused by the radiation defects per strip, which is very important considering that the detectors are exposed to heavy ion beams of high intensity.

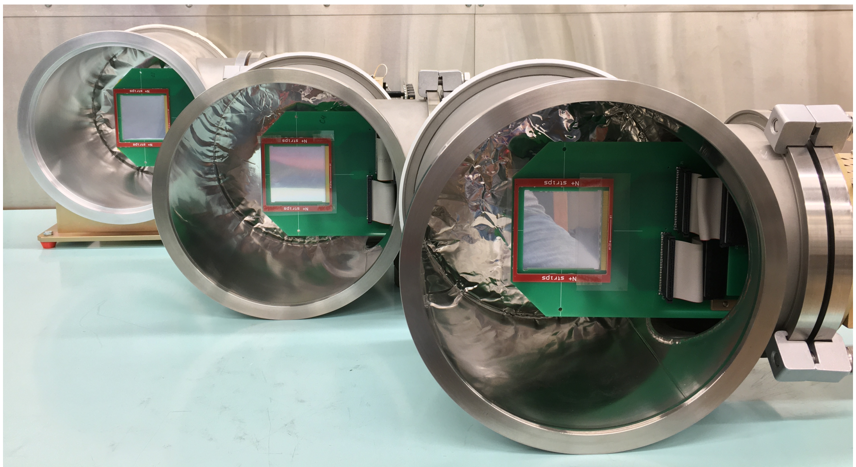

Figure 11: Three stations SiBT1, SiBT2, SiBT3 with detectors and FEE electronics, view along the beam (p^+ side of the strips).

The active area in each of the detectors is $(61 \times 61) mm^2$, and the pitch between strips is 470 μm on both, p+ and n+, sides resulting in total 2 x 128 readout channels. The strips on two sides are oriented orthogonally with respect to each other. The silicon plate in the SiBT1 detector is positioned inside the beam pipe such that the strips are aligned along the X and Y axes, whereas the plates of the SiBT2 and SiBT3 detectors are rotated azimuthally by 30 and 60 degrees respectively.

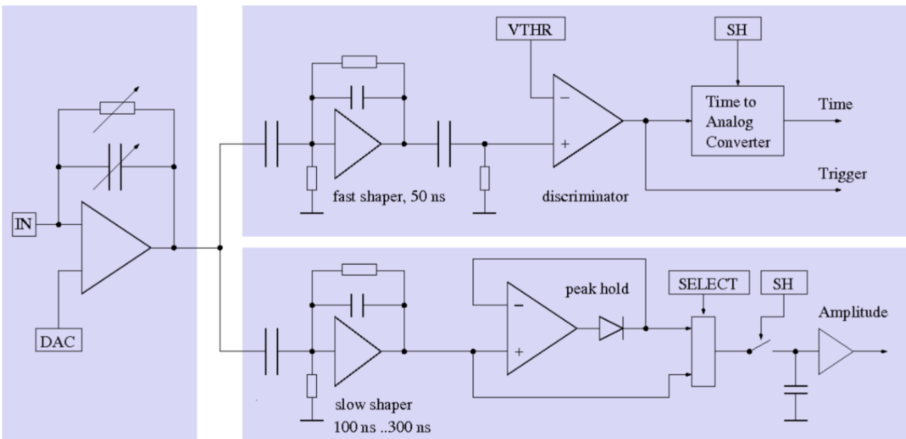

Figure 12: Block diagram of the VATA64HDR16.2 chip for the detector electronics of the beam tracker.

Figure 11 shows three vacuum stations with DSSD coordinate planes installed inside. The positions of the coordinate system of each DSSD plane relative to the geometrical axis of the beam pipe were measured using a NORGAU NVM II-5040D video meter with an accuracy of $+/-50$ µm. Structurally, the detectors are assembled on printed circuit boards with gold contact pads, which are connected by ultrasonic bonding with Al-plated strips on the DSSD surface. The signals from the detector strips in four groups of 64 channels are sent via flat cables to vacuum connectors (4 connectors) fixed in the vacuum flange. The front-end-electronics (FEE) for 128 p^+ and 128 n^+ strips is mounted on the flange outside the vacuum volume. The detector electronics in this case is practically outside of high radiation zone and is available for testing and, if needed, replacement without breaking the vacuum in the beam pipe.

Figure 12 shows a block diagram of the integrated circuit VATA64HDR16.2 (IDEAS, Norway), chosen for the FEE because of its large dynamic range ($-20pC \div +50pC$) suitable for operation with beams of highly ionizing heavy ions. For example, charge in the input signal caused by 3-4 GeV/nucleon Xe ion going through a 175 μm layer of silicon is 11 pC.

The ASIC VATA64HDR16.2 accepts up to 64 input channels, therefore, four of the chips are used in each of the SiBT stations. After passing through pulse shapers, at the time defined by "external trigger - SH", the values of signal amplitudes from 64 strips are stored on the memory capacitors. After that, in sequential reading mode using an analog multiplexer, the 64 signals are transmitted for digitization into a single ADC channel. The main parameters of the VATA64HDR16.2 chip are given in Table 2.

Number of channels	64
Input charge dynamic range	-20pC $\div$ +50pC
Read-out signal generation time	50ns, 100ns, 150ns, 300ns, programmable
Trigger	1 trigger output (Trigger-OR)
Trigger signal generation time	50ns
Equivalent Noise Charge (ENC)	1fC without load
Adjustable trigger threshold	External + 4-bit threshold trim-DAC/ch.
Gain	2-gain settings, programmable
Output	Single analog multiplexed output of 64 pulse height samples
Power consumption per ASIC	960mW max. depending on settings
Voltage supply	+2.5V, -2.5V

Table 2: Main parameters of VATA64HDR16.2 chip.

Figure 13 illustrates three stations of the beam tracker mounted in the vacuum beam pipe of the BM@N channel. Histograms shown at the bottom part of the figure represent online monitoring of 2D distribution of beam ion hits in the tracker. Typical RMS of beam profile in the 2023 Xe run, measured for trigger selected events, i.e. for ions passing through the 2.5 cm dia. hole of the Veto Counter, was 0.5 cm and 0.6 cm in X and Y coordinates respectively.

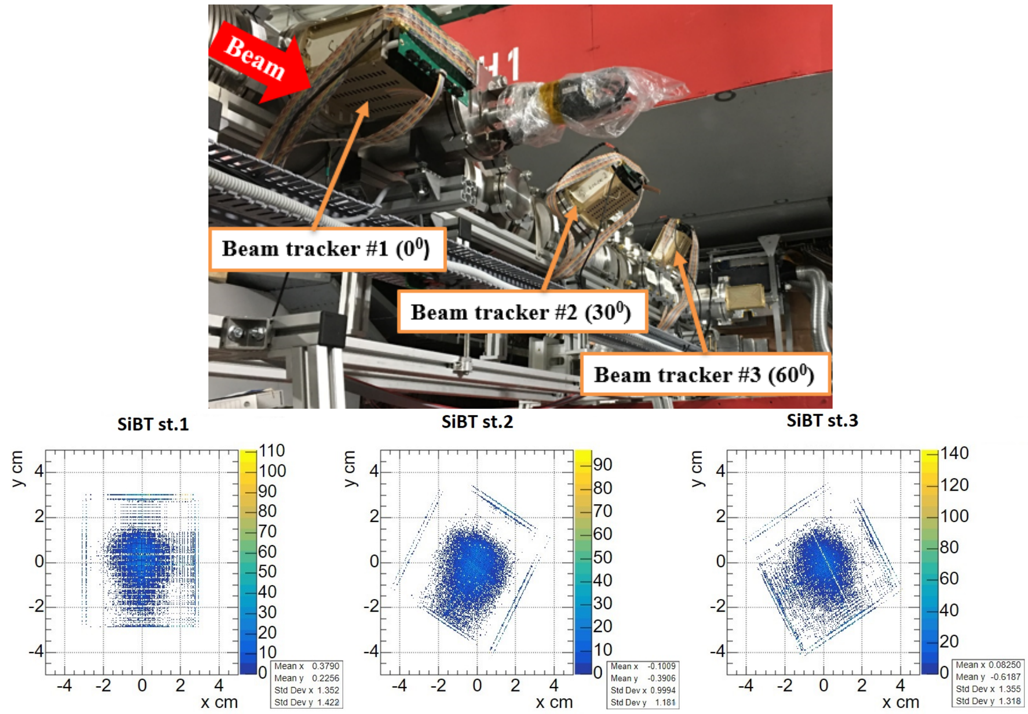

Figure 13. Operating position of three stations of the beam tracker on the vacuum beam pipe of the BM@N channel and two-dimensional beam profiles of Xe (3.8 GeV/n) nuclei measured by the corresponding BT stations.

5 Forward Silicon Detector

Two large tracking detector systems placed inside the analysing magnet are the Forward Silicon Detector (FSD) located right behind the target area, and a set of GEM detectors installed downstream, inside the interpole volume. FSD provides four tracking planes, while the GEM system consists of seven tracking planes. In order to accommodate the beam vacuum pipe going through the setup, each tracking plane in both systems is sub-divided in two half-plane detectors, upper and lower. This section describes the details of the FSD.

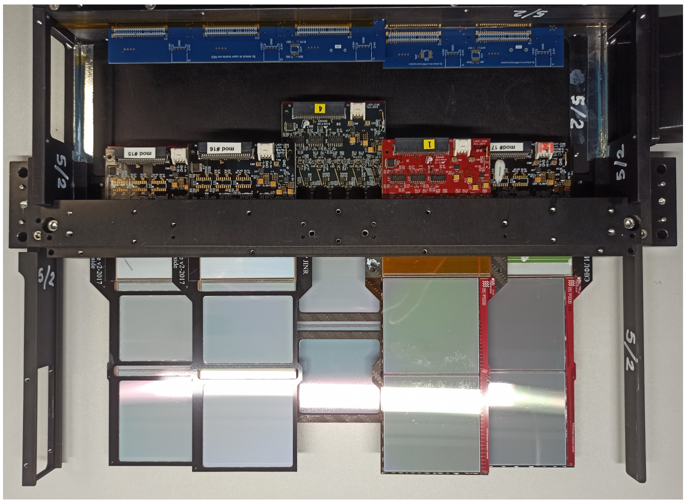

Figure 14: Appearance of the assembled 4 FSD planes (without cables) on the BM@N experiment channel inside the SP-41 analyzing magnet with the beam tube and target assembly installed.

Each half-plane of the FSD forms an independent coordinate detector with the following systems: coordinate modules based on DSSD, electronics backplane, suspension and precise positioning mechanics, cable patch panel, air cooling, temperature monitors, light and EM shield. Top and bottom halves of each plane are made structurally identical and interchangeable. In addition, the design allows vertical shift of the half-planes during the assembly in order to provide possibility to mount / dismount the planes regardless of the installed beam pipe and to minimize probability of its mechanical damage. In the working position, the upper and lower half-planes form a single coordinate system with active regions overlapping along the Y-coordinate. In the center of each plane there is an insensitive 52×52 mm^2 zone (larger ???) which makes room for the beam pipe. The general view of the assembled eight half-planes around the beam tube inside the SP-41 magnet is shown in Fig. 14.

The first plane consists of 6 modules each of which uses one DSSD with dimensions of $(93 \times 63 \times 0.32)$ mm^2 positioned in such a way that the long side is aligned with the Y coordinate. The detector modules of the remaining three coordinate planes use two $(63 \times 63 \times 0.32)$ mm^3 DSSD mounted on a common frame with an accuracy of ($\pm$ 20 μm), where the strips of the same type of one DSSD are connected to the strips of another DSSD by ultrasonic bonding (US-bonding) with an Al-wire $\oslash$ 25 μm. Figure **??** shows the position and coordinates of the Si detectors relative to the target and the axis of the beam pipe, while Table 3 provides information about the number of modules and electronic components in each FSD plane.

The $(63 \times 63 \times 0.32)$ mm^3 and $(93 \times 63 \times 0.32)$ mm^3 DSSDs were manufactured at RIMST (Zelenograd, Russia) and ZNTC (Zelenograd, Russia) respectively. The detectors were cut from 10" and 15" high-resistance mono-crystalline silicon wafers produced by the Float Zone method (ρ >5 k$\Omega\times$cm). Each side, p$^+$ and n$^+$, contain 640 strips, the strip spacing is 95 and 103 μm, respectively, and the relative angle between the strips on two sides is 2.5°. The detectors are positioned in such a way that the strips of the p$^+$ side are aligned with the Y-axis.

Figure 15 shows the external view of the coordinate module with two DSSDs and a demonstration of US-bonding. The diagram of the signal input into FEE is presented in Figure 16. The detector topology (DC) does not contain integrated bias resistors and capacitors for DC decoupling of the strips from the inputs of the readout electronics. The role of the RC-bias element in the DC circuit is performed by the integrated Pitch-Adapter (PA), which also performs the matching of the strip pitch with the pad topology of inputs in the FEE ASIC. Manufactured also at ZNTC, the PAs were made on the basis of Silicon On Sapphire structure. Each PA has 640 RC channels with 1MΩ polysilicon bias resistors and 120pF/100V integral capacitors. The PA-640 integrated

Parameters	1st plane	2nd plane	3rd plane	4th plane	Total
Number of Si- modules	6	10	14	18	48
Number of DSSDs	6 (93 × 63)mm^2	20 (63 × 63)mm^2	28 (63 × 63)mm^2	36 (63 × 63)mm^2	90
Number of ASICs ($T \leq +25°$)	60	100	140	180	480
Dissipated power, W	16.86	28.16	39.42	50.69	135.13
Number of PAs	12	20	28	36	96
Number of FEE PCBs	12	20	28	36	96
Number of channels	7680	12800	17920	23040	53760
Area, m^2	0.035	0.073	0.102	0.132	0.307

Table 3: Main parameters of Forward Silicon Detector BM@N

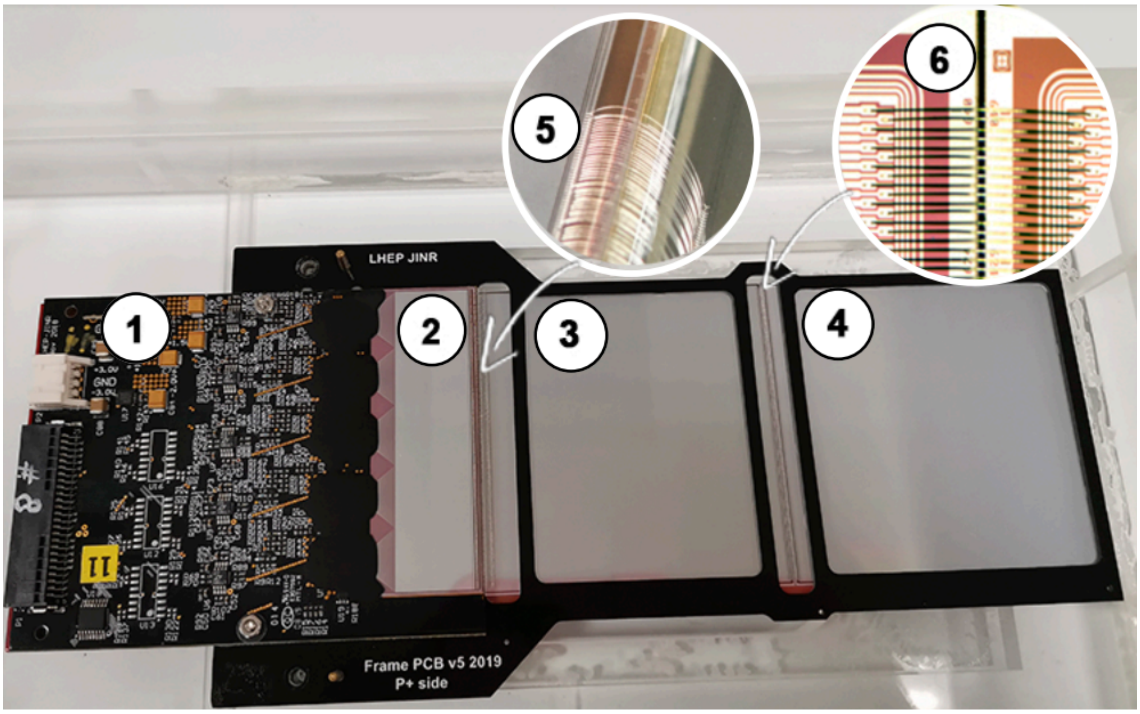

Figure 15: Example of two-way connection US – 2 – x DSSD on the FSD BM@N coordinate module: 1. Read-out electronics. 2. Peach Adapter. 3. DSSD1. 4. DSSD2. 5. Example of US - bonding PA + DSSD1. 6. Example of US - bonding DSSD1 + DSSD2.

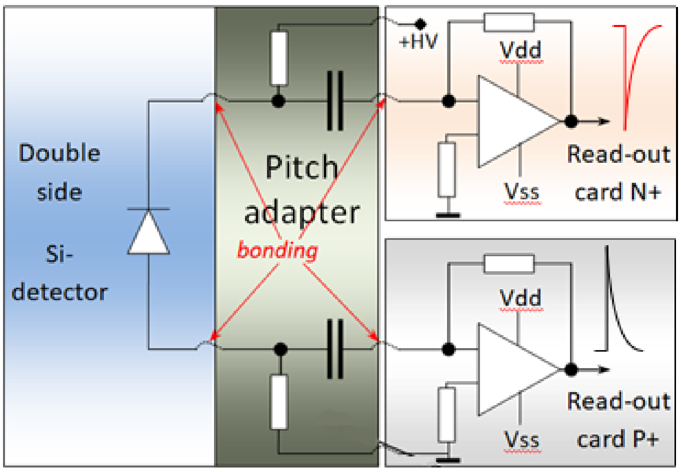

Figure 16: Functional diagram for reading signals from a silicon detector in a coordinate module

circuits have low leakage currents (less than 10-12 A/capacitor/100 V) and an electrical breakdown value of 150 V, which corresponds to electrical intensity in the capacitor of more than 3 MV/cm.

After passing the PA, the signals from the p^+ and n^+ strips of the detector are fed to the inputs of a 128-channel specialized integrated circuit VATAGP7.2 (IDEAS, Norway). (Is it VATAGP7.1 or VATAGP7.2 ???). Each electronic registration channel has a charging amplifier (σ - 200 e), a pulse shaper (peaking time $t_s = 500$ ns), and a memory capacitor which stores pulse amplitude at the trigger time. The ASIC also uses an analog multiplexer channeling 128 inputs to 1 output sent to the read-out in the DAQ by ADC. Two printed circuit bards are used in each FSD module in order to accommodate its input signals, one for 640 negative polarity signals from n^+ strips, the other for 640 positive polarity signals from p^+ strips. Correspondingly, 5 ASICs are mounted on each PCB, welded into the pitch adapters and sealed with a compound.

After the assembly of the modules in a half-plane, the position and rotation angles of every DSSD with respect to geodetic markers on the half-plane housing is measured using the NORGAU NVM II-5040D video meter with an accuracy of ± 50 μm. The markers are subsequently used during the installation in order to bind the position of each detector to the common coordinate system of the experimental setup.

Fig. 17 illustrates distribution of hits in the 4th plane of the FSD observed in the 2023 Xe run. Dark bands in the distribution indicate insensitive groups of 128 channels (1 chip). Number of such faulty chips at the end of the run was equal to 0, 1, 1, 8 for the 1st, 2nd, 3rd and 4th planes, respectively, which corresponds to 0, 1.0, 0.7 and 4.4 % of the channels. This malfunction can be due to the following reasons: 1) broken electrical contact in the transmission circuit from the chip (FEE buffer, cross-board connector, patch panel cable, long ADC-64 cable) 2) failure of the chip (no programming of the operating mode) or breakage of the US-bonding. Defects of the first type can be repaired, while the failings in the second group are of a permanent nature.

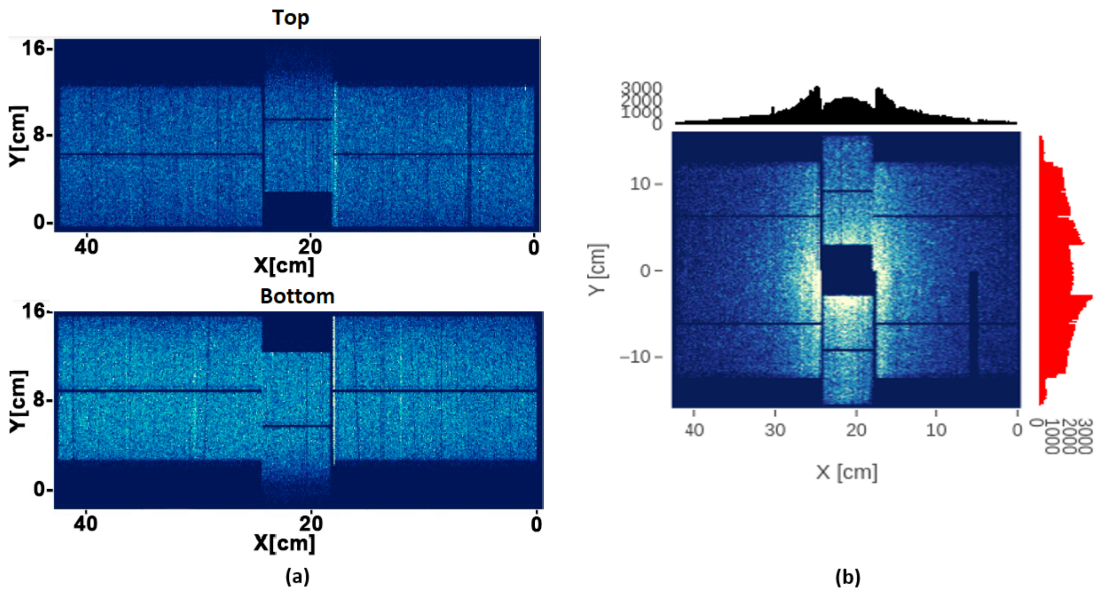

Figure 17: Comparative data on channel occupancy in space tests (a) and in Session BM@N (2022-2023) RUN # 7529 (11.01.2023), $t_c = 25.2°$C, Target #2 CsI (2%) (b).

6 GEM

Central tracking system is based on Triple-GEM detectors located inside the analysing magnet SP-41 downstream the FSD. Full configuration of the GEM tracking system implemented in the 2023 Xe run consists of 14 detectors forming 7 tracking planes: 7 top detectors above the vacuum beam pipe, and 7 bottom detectors below the pipe. Because the beam line inside the SP-41 goes closer to the bottom pole of the magnet, in order to cover the maximum possible acceptance, the top and bottom detectors have been designed with different active area sizes, 163×45 cm^2 and 163×39 cm^2, respectively.

6.1 GEM construction

The BM@N GEM detectors were produced using non-glue ”foil-stretching” technology and assembled at CERN in the PH Detector Technologies and Micro-Pattern Technologies workshop. All three GEM foils in a detector are identical and made of a 50 μm Kapton covered on both sides with 5 μm copper electrodes. Foils are perforated by holes of about 70 μm diameter, separated by a distance of 140 μm. The gaps between the electrodes are shown in Fig. 18 (left).

The anode plane is used for the readout and organized as a multilayered board with two types of parallel strips: aligned with the vertical axis and inclined by 15 degrees with respect to it, as shown in Fig. 18 (right). The width of vertical and inclined strips is 680 μm and 160 μm respectively, while the pitch for both types of strips is 800 μm. The readout plane is subdivided by two halves and, in addition, separate readout is organized for the region close to the beam pipe where higher density of hits is expected. The size of this ”hot zone” is approximately 80×15 cm^2. The readout FEE boards are mounted on the frames of the detectors outside of the acceptance. More details on the design, tests and preparation of the detectors can be found in [13, 14].

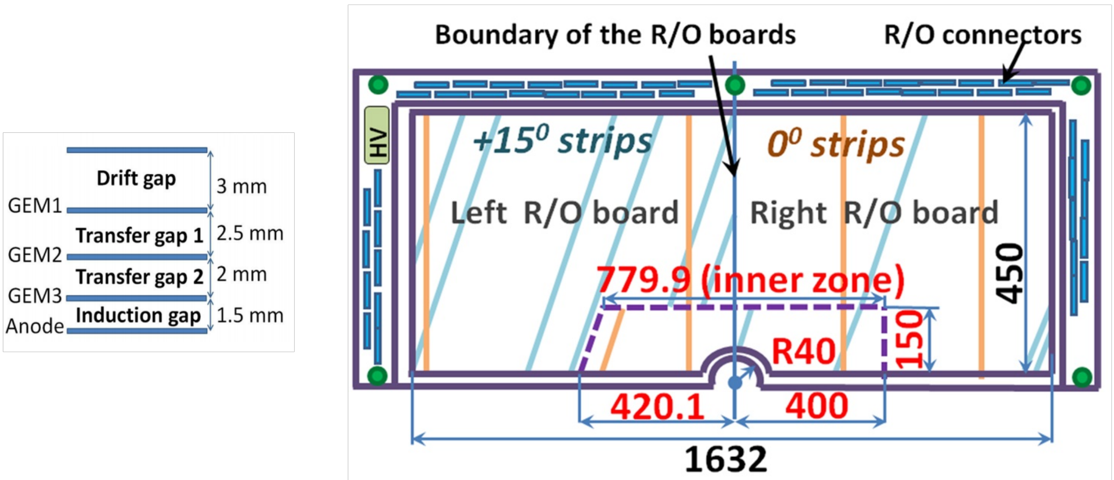

Figure 18: Design of the detectors: cross-section of triple GEM (left); schematic view of the top detector (right).

6.2 Mechanical support

The position and configuration of GEM detectors in the 2023 Xe run is shown in Fig. 19 and Fig. 20.

The mechanical support of the GEM detectors inside the SP-41 magnet was designed and manufactured by LLC “Pelcom Dubna Machine-Building Plant”. The support structure is made of non-magnetic material and satisfies strict requirements for precise positioning of the detectors. The weight of one GEM detector equipped with mechanics, front-end electronics and cables is about 19.5 kg. The whole assembly of 14 GEM detectors during the installation can be vertically

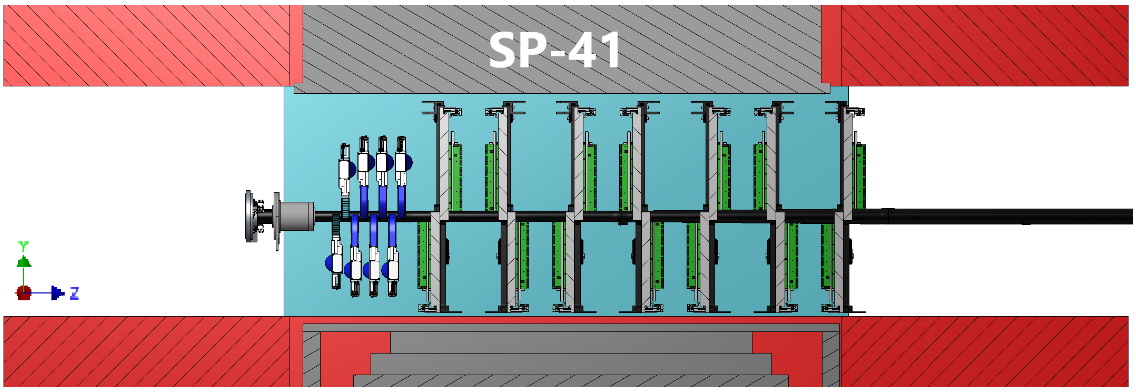

Figure 19: The position of GEM detector package relative to the magnet coil

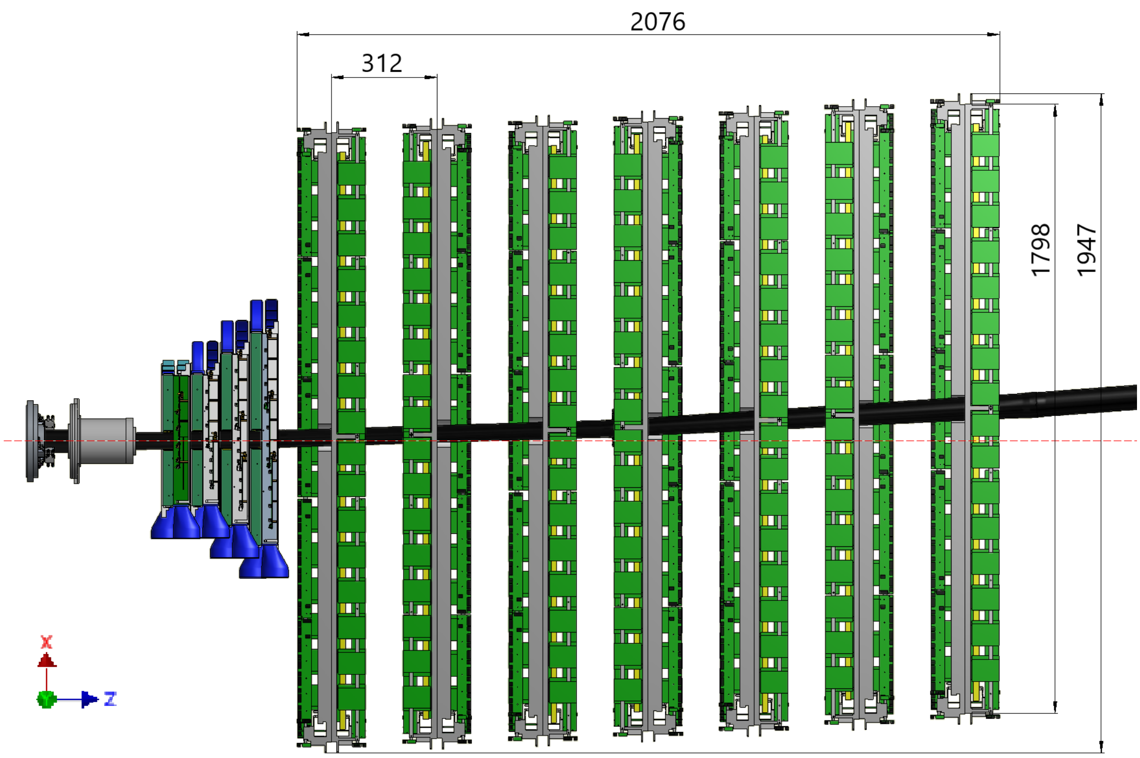

Figure 20: Displacement of detectors relative to each other due to beam pipe bending

adjusted by $\pm$10mm relative to the surface of the magnet coil. In addition, the setup allows to shift each GEM detector vertically by $\pm$5 mm with respect to the mechanical support. The accuracy of positioning of each detector relative to the other (one half-plane relative to the other half-plane ?) does not not exceed 0.5 mm. After the installation and alignment of each detector, the coordinates of the frame corners and the center of the semi-circular notch for the beam pipe are measured with an accuracy better than xxx.

Installation of the detectors includes the following steps: 1) bottom detectors are installed sequentially, starting from the detector closest to the target; 2) a carbon beam pipe is installed on top of the bottom detectors; 3) top detectors are installed sequentially, starting from the detector closest to the target. Photo of the installation process is shown in Fig. 21.

Prior to the installation the detectors were tested with cosmic muons in order to determine uniformity of the gain in different regions. Lower amplification in the outer parts of the detectors was observed, with typical variation in the range $\pm$20%. During the installation, the detectors, which, due to this effect, can have lower efficiency in the side parts, were placed closer to the target, where outer regions are less significant for track reconstruction.

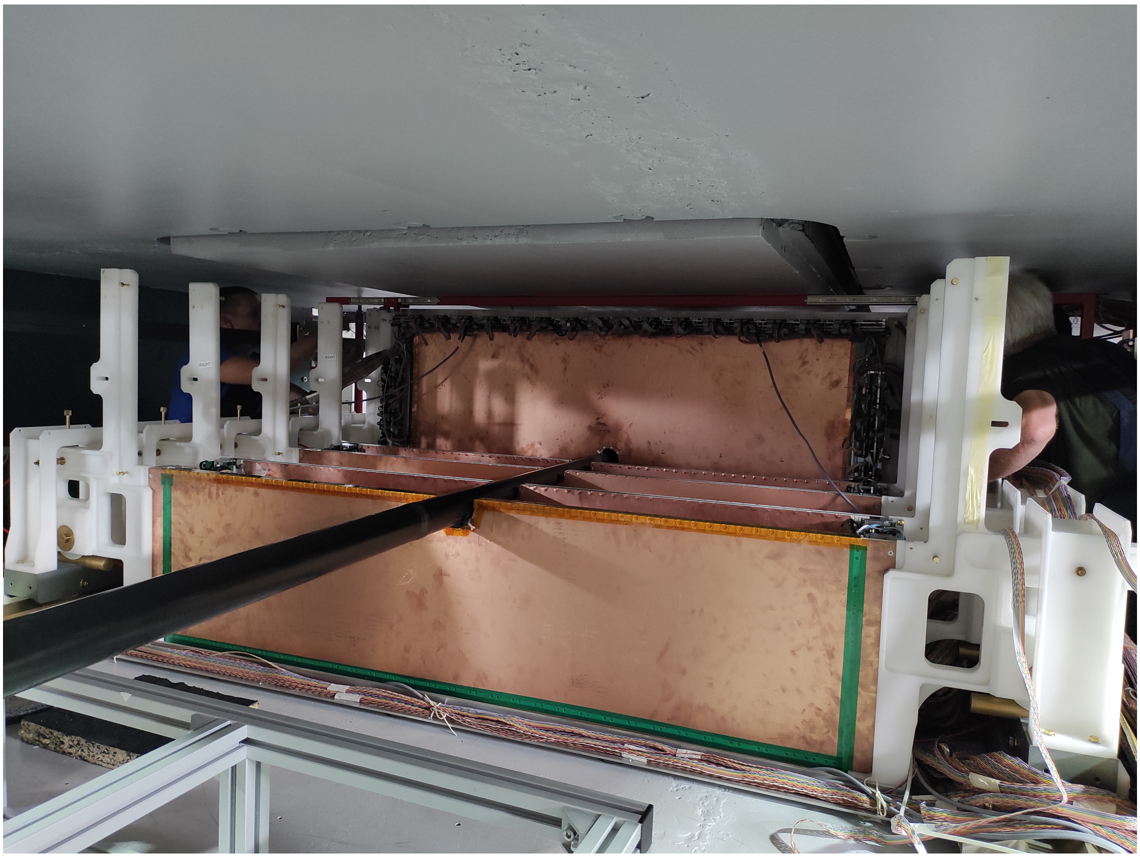

Figure 21: Photo of GEM detectors installation from back side of SP-41 magnet (in the direction opposite to the beam)

6.3 Gas system

Ar(80)C_4H_{20}(10) gas mixture was chosen for the operation in the 2023 Xe run, while the overall GEM amplification was maintained at the level of 3×10^4. The H_2O and O_2 removal filter was installed in the gas system after the gas mixer. The gas line is divided into two identical lines for independent connection of the top and bottom GEM detectors. Two rotameters were installed in the lines, allowing to regulate the gas flow. Each line connected a group of top or bottom detectors in series, starting with the detector closest to the target. The small GEM detector (see the section "Beam and trigger detectors") was connected last in the line for the bottom detectors. The gas flow rate in each line during the 2023 Xe run was at the level of 3 l/h.

6.4 Front-end electronics

Front-end electronics is based on the 32-channel integrated circuit VA163 (IDEAS, Norway). Each channel of the ASIC has a charge sensitive pre-amplifier, a shaper with 2 μs peaking time, and a sample holder circuit. An analog multiplexer sends channel by channel 32 sampled signals into one serial read-out. Four ASICs are joined in one front-end board. The multiplexed data from each board are transmitted through 13m of twisted pair flat cable to the 12-bit analog-to-digital converter. More detailed description of the FEE can be found in [15].

7 TOF

(*RumyantsevM.mikhail.rumyantsev@yandex.ru*)

For charge particle identification the two Time-of-flight systems are used in BM@N. The first TOF system is placed at about 4 meters from the target and looks like two arms to the left and right of beam axis (TOF-400). The second TOF wall (TOF-700) is located at a distance of 7 meters from the target (fig 1). The arrangement of both systems provides continuous geometric acceptance and overlap with the external track systems. The basic requirements to the TOF system are:

- high granularity to keep the overall system occupancy below 15% and minimize efficiency degradation due to double hits;
- good position resolution to provide effective matching of TOF hits with tracks;
- high combined geometrical and detection efficiency (better than 85%);
- identification of pions and kaons with 0.1 < p_t < 3 GeV/c;
- identification of (anti)protons with 0.3 < p_t < 5 GeV/c

To achieve these goals, a strip-readable Multigap Resistive Plate Chamber (MRPC) detector was chosen for both TOF systems. This type of detectors is widely used for time-of-flight measurements (ref....). It showed good efficiency, high time resolution, the ability to work with particles flux up to tens kHz/cm^2.

7.1 TOF400

The TOF400 system consists of two part are placed left and right to the beam. Every part consist of two gas boxes (modules) with 5 MRPCs each 22. The active area of the MRPCs overlap on 50 mm inside the box. Gas box made from aluminum frame covered by aluminum honeycomb for reduction of radiation length. Overlap of gas boxes ensures crossing of active area of detectors 50 mm also. Active area of every part is 1.10x1.3 m^2 and defined to satisfy the geometrical acceptance of the GEM tracking detectors. The main parameters of the TOF400 are present in Table 5.

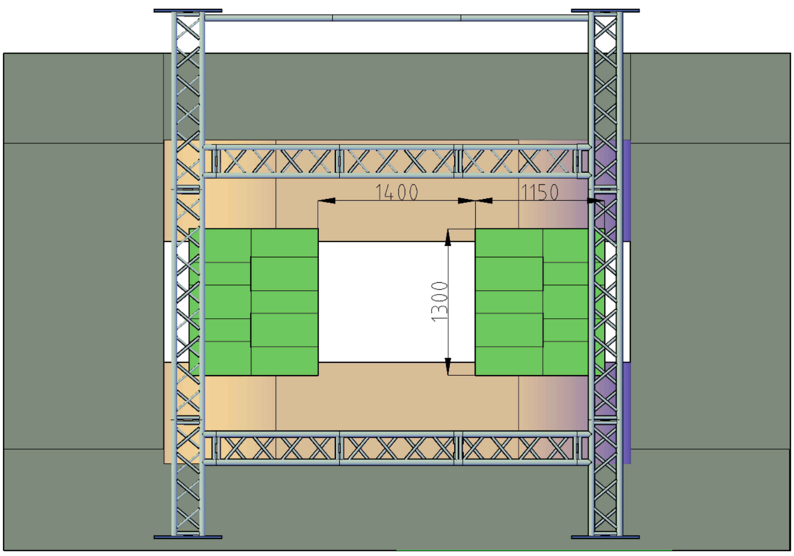

Figure 22: Schematic view of TOF400 system

A scheme of MRPC for TOF400 system is shown on Fig. 28. The detector consists of three stacks of 5 gas gaps each. Float glass with a thickness of 420 μm for external electrodes of the stack and 240 μm for internal ones was used as resistive electrodes. The fishing line as a spacer defines the 200 μm gap between all resistive electrodes. The outer part of external glass electrodes is covered by conductive paint with surface resistivity about 2-10 M$\Omega/\square$ to apply high voltage. All internal glasses are floating. The pickup electrodes look like strips and made on the PCB board. The main feature of the proposed triple-stack MRPC is that readout strips are located only in the

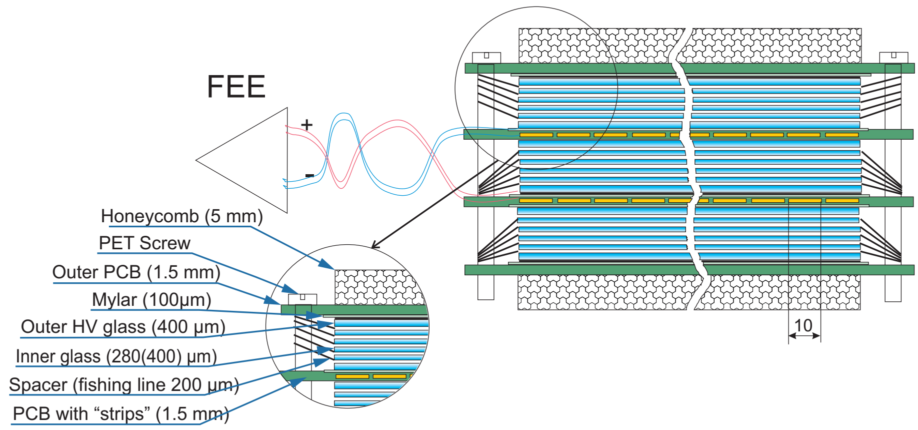

Figure 23: Schematic view of the MRPC detector for TOF400 system

inner stack. This ensures that the construction is symmetric, and speed of signals on the anode and cathode are the same, what prevent the dispersion of the signal. Differential analog signal from strip is transferred by twisted pair cable to front-end electronics. Signal is reading out from both ends of the strip. It provides better time resolution and determination of the coordinate of a particle along the strip. For stiffening structure we glue paper honeycomb with a thickness of 10 mm on outer part of the external PCBs. Dimension of active area of one MRPC is 300*600 mm^2. It has 48 readout strips, 10 mm wide and 300 mm long. To reduce crosstalk the gap between strips is 2.5 mm. Thus the pitch of electrodes in this case is 12.5 mm.

The charge sensitive NINO chip was used for TOF400 []. The chip has 8 channels and processed on 0.25 μm technology. Each channel includes ultra-fast preamplifier with a peaking time less than 1 ns, discriminator with a minimum detection threshold of 10 fC and output stage which provides LVDS output signal. The duration of the LVDS signal is proportional to the charge of the input signal, so it can be used for so-called amplitude-time correction. The 24-channel amplifier-discriminator base on NINO chip was developed in LHEP JINR []. Measurements with a test signal from the generator showed an intrinsic time resolution of the amplifier of 7 ps. The amplifier are placed as close to the MRPC as possible on front cover of the gas box. The signal from the preamplifier can be transmitted over a distance of up to 10 m via a special cable without loss of time resolution. Additional features of the FEE are the ability to remotely control the threshold, measure the supply voltage and temperature on the board via the RS485 interface.

72-channel time-to-digital converters (TDC72VHL []) based on HPTDC chip [] were developed in LHEP JINR for digitization of LVDS signals and data acquisition. The TDC72VHL operates in ultra high resolution mode with a bining of 23.4 ps. This allows to measure the leading and trailing edges of the input LVDS signal with high accuracy, but there is significant integral non-linearity at the TDC. This nonlinearity causes strong degradation of time resolution. The method of uniform filling the time gap with random events (code density test) was used for calibration (consideration of nonlinearity) of TDC module. The intrinsic time resolution of an individual TDC72VHL channel averaged 20 ps after applying the calibrations.

The prototype of full scale MRPC with full readout chain was tested on the Nuclotron beam at LHEP. The deuteron beam was transferred to the experimental setup "Test MPD" []. The fast Cherencove counter [] with time resolution of 37 ps was used as a start detector. The result of measuring the efficiency and time resolution are present on the Fig. 29a . All results include contributions from the front end and data acquisition electronics. The efficiency is higher than 98% and time resolution is below 50 ps for different threshold of NINO. A voltage of 11.5 kV and a threshold of 120 mV were chosen as the operating point. Results of high rate test are presented on Fig. 29b. MC simulations show that the particle flux on the TOF400 does not exceed 1 kHz/cm2, so a time resolution of less than 50 ps and an efficiency of more than 95% are expected.

7.2 TOF700

The TOF700 wall placed at about 7 meters from the target and made of MRPC of different size in an individual gas box each. The wall size of 3.2x2.2 m^2 is defined to satisfy the geometrical acceptance of the outer tracking detectors (DCH). The detectors are mounted on two subwalls in two layers on each to provide a geometric overlap between the detectors. Both sub walls can move relative to each other to provide access for installation and maintenance. Two types of detectors

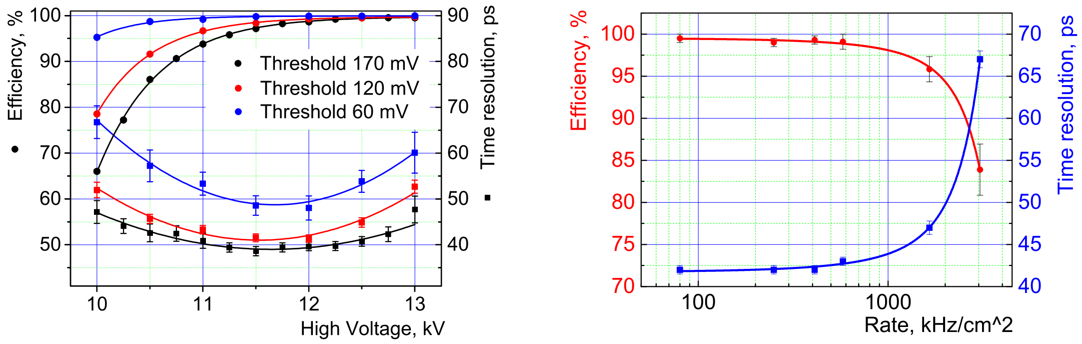

(a) (b)

Figure 24: Performance of the MRPC designed for TOF400 system. The detector efficiency and time resolution as function of applied of HV for different NINO thresholds are shown on the left. The right shows the dependence of the detector performance on the particle flux for 11.5 kV and 120 mv threshold.

are used for TOF700: a "cold" MRPC with an active area of 30.3x56 cm^2 (16 strips of 18x560 mm^2) for the area with a low particle flux and a "warm" MRPC with an active area of 16x35.1 cm^2 (32 strips 10x160 mm^2) for the area near the beam line. The main parameters of the TOF700 are present in Table 5.

A schematic cross-section of a "cold" MRPC is shown in Fig. 31. It consists of two identical stacks with five gaps each. Each stack is formed by six glass plates 0.67 mm thick with the bulk resistivity of 2x10^{1}2 $\Omega\times$cm. The gap between the glasses 0.3 mm is fixed by spacers (fishing-lines). Graphite conductive coating with surface resistivity of 1 M$\Omega/\Box$ is painted to outer surfaces of external glass plates to distribute both the high voltage and its ground. The anode readout plate is a 100 $/mu$m one-sided printed PCB and is placed between stacks. Unipolar signals are taken from both ends of the reading strips, which makes it possible to determine the coordinate of the particle along the strip. Each detector is placed in an individual gas box. The bottom cover is made of PCB 2.5 mm thick and is designed to take out a signal from the box volume to readout electronics. The frame of the box is made of aluminum 2.5 mm thick. The top cover is made of 1.5 mm thick aluminum sheet. The box covers are reference plan for a unipolar signal. Warm MRPC is built in the same way as cold mRPC. However to increase the ate capability the gas gaps and the thickness of the glass plates are reduced (0.22 mm and 0.55 mm respectively). To compensate for the loss of the signal amplitude due to the increasing of the anode strip-cathode capacity, the number of gaps in the chamber was increased from 10 to 12 (six gaps per stack).

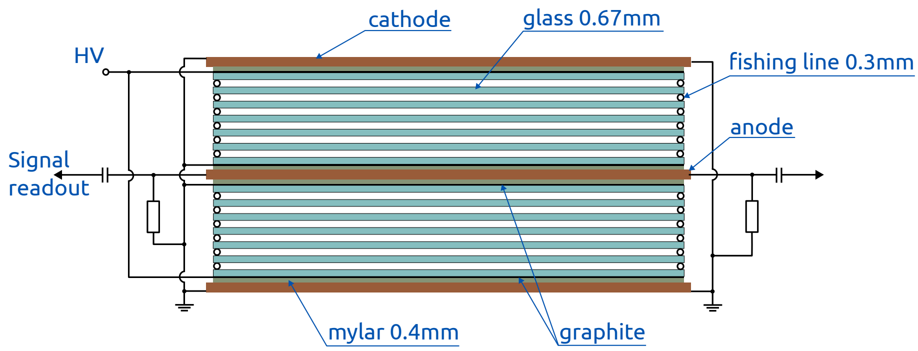

Figure 25: Schematic view of the MRPC detector for TOF700 system

The AddOn board base on NINO chip developed for the HADES experiment was chosen as front-end electronics (FEE) for TOF700. Signals from the MRPC to the FEE (32RPC) are received over 50 ohm coaxial cables using MMCX connectors. The LVDS output signals are transmitted to the digitizing module using DHR-78F connectors. A 64-channel VME TDC64VHLE time-to-digital converter based on the HPTDC chip is used for digitization. With a special module (PWR&CTRL) it is possible to remotely control the power supply, the discrimination threshold and hysteresis value on the FEE.

Prototypes of "cold" and "warm" detectors were tested on the secondary muon beam of the U-70 accelerator at IHEP. The test was carried out on the "MUON" facility with a particle flux of about 1 kHz/cm^2. A fast scintillation counter with its own time resolution of 40 ps was used as T0. The test results of both prototypes are shown in the figure 32. The intrinsic time resolution of the MRPCs with electronics is better than 45 ps with an efficiency of 98% and 95% for "cold" and "warm" chambers respectively.

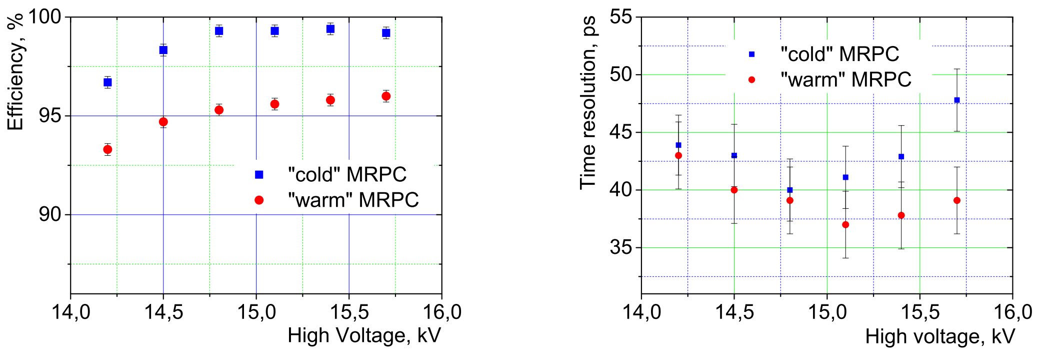

(a) (b)

Figure 26: Performance of the MRPC designed for TOF700 system. The detectors efficiency are shown on the left and time resolution are shown on the right.

	TOF400	TOF700
MRPC active area	30x60 cm^2	30.3x56 cm^2 "cold" 16x35.1 cm^2 "warm"
FEE on one MRPC	96	32 for "cold" 64 for "warm"
Number of MRPC	20	30 "cold" 40 "warm"
Total active area	2 Arms x 1.1x1.3 m^2	3.2x2.2 m^2
Total number of FEE	1920	3520

Table 4: Main parameters of TOF system.

7.3 Services system

Both TOF400 and TOF700 systems use the same a non-flammable Freon rich gas mixture containing 90% C2H2F4 + 5% i-C4H10 + 5% SF6. A simple open-loop gas system was designed for the BMN experiment. This system is based on the MKS 1479A controllers for measuring and adjusting the absolute flow of components with an accuracy of 0.3%. The flow rate of the gas mixture can be adjusted in the range from 6 l/h to 90 l/h, but the typical value is 21 l/h, which corresponds to the exchange of 2 volumes per day. Also, one additional channel is available for purging the system with nitrogen for cleaning and drying. A special PC program has been written to control the parameters of the gas system via the Ethernet interface.

The MRPC detector operates at very high voltage of 12 kV and 15 kV for TOF400 and TOF700 respectively. On the other hand, the dark currents of the detector are quite small at the level of tens of nA. Also, the detector is very sensitive to voltage ripples due to the large capacitive coupling between the high-voltage layer and the readout strips. Therefore, the high-voltage system is subject to high requirements for voltage stability and current measurement accuracy. The high-voltage power supply systems for both TOF are based on commercially available ISeg modules and a specially designed HVSys power supply. All elements of the system have the ability to remotely control via Ethernet interface.

To monitor of stability of operation of the TOF systems all controlled parameters are sent to the Slow Control System. The data is displayed on the website of the experiment via Grafana. The operator can see the value of the high voltage and current on the detectors, the set voltages and thresholds of the amplifiers, the gas flow and the weight of the gas in cylinders, and other parameters. In case of an emergency, the operator receives a message that allows to respond in time. All data is stored in a database and can be used for further analysis.

8 TOF v2

Two time-of-flight systems are used in BM@N for charge particle identification. The first system, TOF-400, is placed at about 4 meters from the target and consists of two arms to the left and right of the beam axis. The second, TOF-700, is located at a distance of about 7 meters from the target. The arrangement of both systems provides continuous geometric acceptance and overlap with the FSD, GEM and outer tracking systems. Choice of detectors and their parameters was dictated by the following requirements:

- high granularity and rate capability, which would allow to keep the overall system occupancy below 15% and minimize efficiency degradation due to double hits;
- good position resolution in order to provide effective matching of TOF hits with tracks;
- high combined geometrical and detection efficiency (better than 85%);
- separation of pions and kaons in the momentum range $0.1 < p < 3$ GeV/c;
- separation of kaons and protons in the momentum range $0.3 < p < 5$ GeV/c.

To achieve necessary performance, a strip-readable Multigap Resistive Plate Chamber (MRPC) detector was chosen for both TOF sub-systems. This type of detectors is widely used for time-of-flight measurements. It showed good efficiency, excellent time resolution, ability to work with particle flux up to tens kHz/cm^2.

8.1 TOF400

Left and right arms of the TOF400 system are placed symmetrically with respect to the beam. Every part consists of two gas boxes (modules) each having 5 MRPC detectors 27. The active area of one detector is 60x30 cm^2. Inside the box, active areas of adjacent detectors overlap vertically by 50 mm, while horizontal overlap of the gas boxes ensures crossing of active area of detectors by 50 mm as well, which makes total active area of each of the two arms to be equal to 1.10x1.3 m^2 matching the geometrical acceptance of the 1x1 m^2 CSC tracking detectors and covering significant fraction of the GEM acceptance. Each gas box is formed by an aluminum frame closed from the front and back sides by aluminum honeycomb plates, which provide sufficient rigidity while having small thickness in radiation lengths.

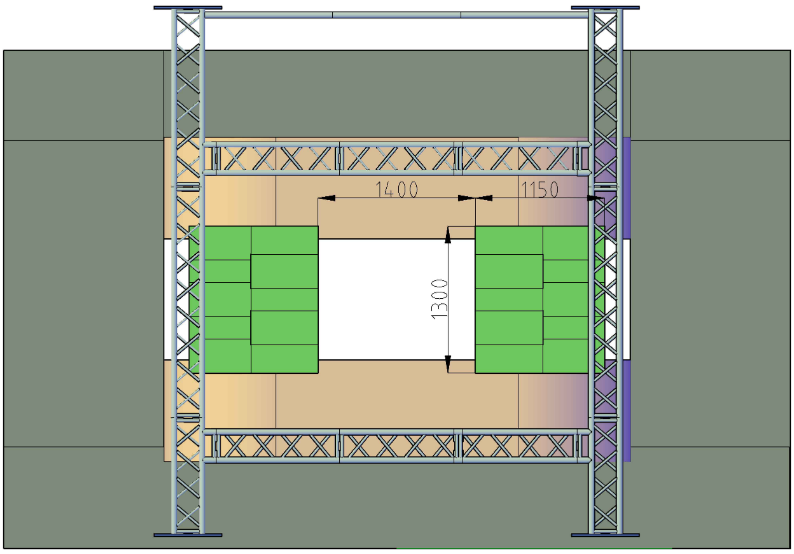

Figure 27: Schematic view of TOF400 system

Fig. 28 shows schematic cross section of the TOF400 MRPC. The detector consists of three stacks inserted between two outer 1.5 mm thick PCBs, and separated by two inner PCBs also 1.5 mm thick. In order to add stiffness to the structure, paper honeycombs with a thickness of 10 mm were glued on the outer sides of the external PCBs. Each stack has 5 gas gaps between

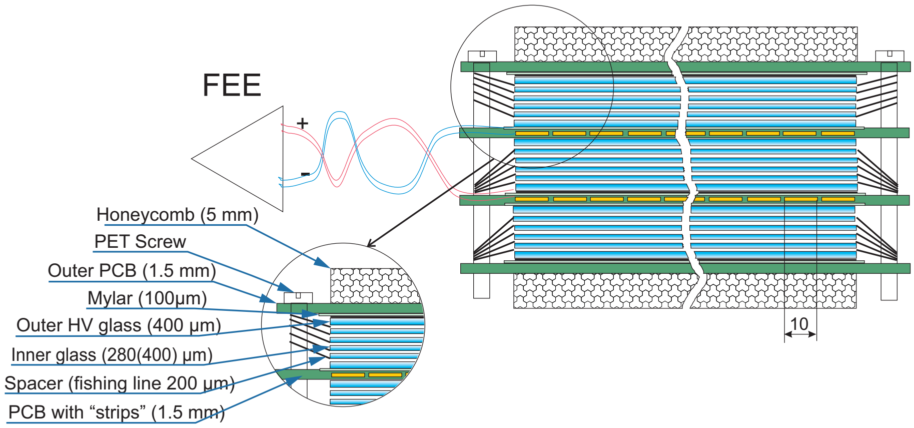

Figure 28: Schematic cross section of TOF400 MRPC

glass sheets which are used as resistive electrodes. Two external glass sheets in a stack have a thickness of 420 μm, while four internal sheets are 240 μm thick (the numbers in the Figure are different Sic!). Fishing line as a spacer defines the 200 μm gap between all the glass plates. High voltage is applied to the outer part of external glass electrodes covered by conductive paint with surface resistivity of about 2-10 MΩ/sq. All internal glass electrodes are left electrically floating. Two PCBs with pickup readout pads are placed on both sides of the inner stack, one serving as the cathode readout plane, the other as the anode one. Correspondingly, the HV is applied in an alternating sequence, as shown on the right side of the Fig. 28, (*** should be added to the picture! ***) in order to form symmetrical configuration for the cathode and anode readout planes. Such a configuration was chosen to ensure that propagation of signals to the FEE has equal speed on positive and negative lines, thus preventing dispersion of the differential signal.

Readout pads have a shape of strips with area of 300x10 mm^2 arranged vertically with 12.5 mm pitch, making 48 readout strips in each of the PCBs. The 2.5 mm gap between the strips is introduced in order to reduce cross talk between adjacent channels. Signals from strips are transferred to the front-end electronics by twisted pair cables. In order to obtain better time resolution and determination of hit coordinate along the strip, the signals are read out from both ends of the strip.

FEE of the TOF400 is based on the NINO amplifier/discriminator ASIC developed in CERN for the time-of-flight system of the ALICE experiment [?]. The chip has 8 input channels and processed on 0.25 μm technology. Each channel includes an ultra-fast preamplifier with peaking time less than 1 ns, a discriminator with a minimum detection threshold of 10 fC and an output stage which provides LVDS output signal. The duration of the LVDS signal is proportional to the charge of the input signal, and can be used for the amplitude-time correction. The 24-channel FEE board, which combines signal processing by three NINO chips, was developed in LHEP JINR [?]. In order to ensure optimal operation of the FEE, the boards are placed as close to the MRPC as possible and mounted on the front cover of the gas box. Measurements with a test signal from the generator showed an intrinsic time resolution of the FEE chain of about 7 ps. Additional features of the FEE board include the ability to remotely control the threshold levels of the NINO discriminators, and to measure the supply voltage and temperature on the board via the RS485 interface.

LVDS signals from the FEE boards are transmitted over a distance of up to 10 m via a special cable without loss of time resolution. The signals are digitized in 72-channel time-to-digital converters (TDC72VHL) based on the HPTDC chip [?]. The TDC72VHL were developed in LHEP JINR and operate in ultra high resolution mode with a bining of 23.4 ps [?]. Such fine binning allows to determine the leading and trailing edges of the input LVDS signals with high accuracy. However, the TDCs exhibit significant integral non-linearity, which, if not corrected, causes significant degradation of the time resolution. The method of uniform filling the TDC time window with random events (code density test) is used for non-linearity calibration of every channel of the TDC module. After applying the non-linearity correction, the intrinsic time resolution of individual TDC72VHL channels is equal to 20 ps on average.

A full scale MRPC prototype with complete readout chain and 90% C2H2F4 + 5% i-C4H10 + 5% SF6 gas mixture was tested in the Nuclotron deutron beam [?]. Fast Cherenkov counter with time resolution of 37 ps was used as a start detector. Measured efficiency and time resolution as a function of high voltage for different levels of the NINO discriminator threshold are presented in the

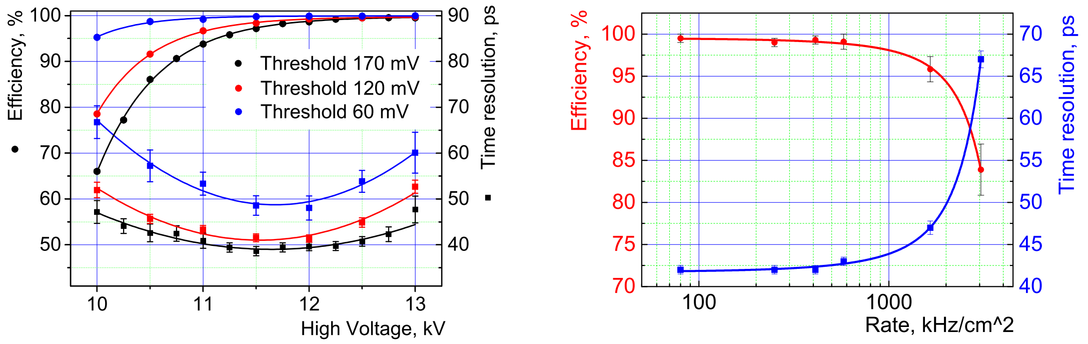

(a) (b)

Figure 29: Performance of the MRPC designed for TOF400 system. The detector efficiency and time resolution as a function of applied of HV for different NINO thresholds are shown on the left. The right plot shows the dependence of the detector performance on the particle flux for 11.5 kV and 120 mv threshold.

Fig. 29a. All the results include contributions from the front-end and data acquisition electronics. Based on the measured prototype performance, high voltage of 11.5 kV and discriminator threshold of 120 mV were chosen as the operating point of the TOF400 modules. With these settings, the dependence of efficiency and time resolution on the particle rate was studied with the prototype, the results of these tests are presented in Fig. 29b. Monte Carlo simulations show that under the BM@N conditions, even at the highest heavy ion beam intensity, the particle flux in the TOF400 does not exceed 1 kHz/cm2, therefore, time resolution better than 50 ps and efficiency higher than 95% are expected.

8.2 TOF700

The TOF700 wall is placed at about 7 meters from the target and has active area of 3.2x2.2 m^2 in X and Y, respectively, defined to overlap with the geometrical acceptance of the outer tracking detectors (DCH and 2.2×1.5 m^2 CSC) as well as to cover significant fraction of the GEM acceptance. At the center of the TOF700 wall there is an opening for the vacuum beam pipe. Because density of hits from particles produces in heavy ion collisions significantly higher in the region close to the beam, two types of MRPC detectors are used for TOF700: ”cold” – with an active area of 30.3x56 cm^2 and 16 readout strips of 18x560 mm^2 for the outer area with a low particle flux, and ”warm” – with an active area of 16x35.1 cm^2 and 32 strips of 10x160 mm^2 for the area near the beam line. Vertical orientation and the size of the readout strips were dictated by expected hit occupancy and the requirement of unambiguous matching of hits with particle tracks. Arrangement of TOF700 MRPCs in the XY plane is shown in 30. The detectors are mounted on two sub-walls, which can slide relative to each other to facilitate access for installation and maintenance of the detectors. In addition, the MRPCs in each sub-wall are arranged in two layers in order to provide possibility for geometrical overlap between adjacent detectors.

”Cold” and ”warm” MRPCs have similar two-stack design with a single anode readout plane placed between the stacks. A schematic cross-section of a ”cold” MRPC is shown in Fig. 31. Each stack is formed by six glass plates 0.67 mm thick with the bulk resistivity of 2x10^{1}2 Ω×cm. Fishing-lines spacers define 0.3 mm gap between the glass sheets. Graphite conductive coating with surface resistivity of 1 MΩ/sq is painted on the outer surfaces of the external glass plates in order to apply both the high voltage and the ground. The anode readout plane is arranged on a 100 $/mum$ one-sided PCB. Unipolar signals are taken from both ends of the strips, which makes it possible to determine the coordinate of the particle hit along the strip by measuring time difference between the signals. Each detector is placed in an individual gas box, which is formed by a 2.5 mm thick aluminum frame and two cover plates. One cover is made of 2.5 mm thick PCB and is designed to take out signal wires from the box volume to the readout electronics. The other cover is made of 1.5 mm thick aluminum sheet.

The design of ”warm” MRPCs has only minor modifications. In order to increase detectors rate capability, the gas gaps and thickness of the glass plates in warm MRPCs are reduced to 0.22 mm and 0.55 mm respectively. Such a reduction leads to lower signal amplitudes due to increased

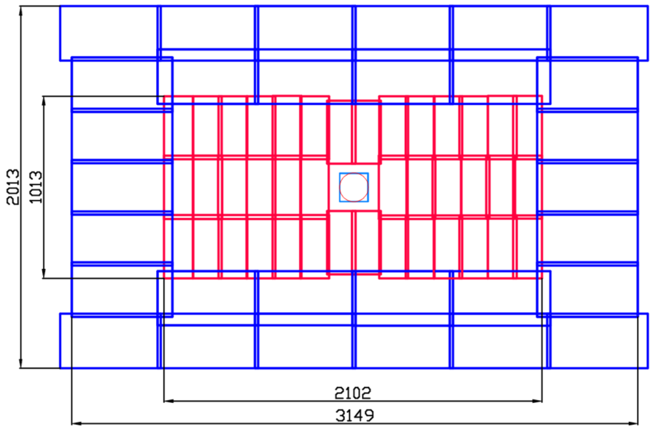

Figure 30: Arrangement 40 "warm" (red) and 32 "cold" (blue) MRPCs in the TOF700 active area.

anode strip-cathode capacity. To compensate for this signal weakening, the number of gaps in the chamber was increased from 10 to 12 (six gaps per stack).

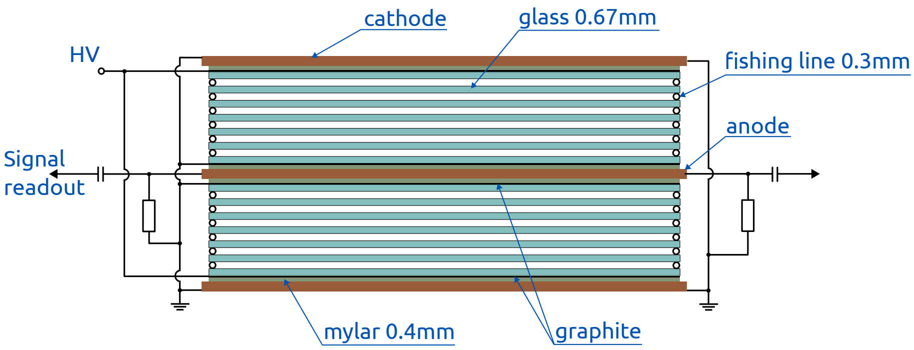

Figure 31: Schematic view of the MRPC detector for TOF700 system

The FEE board developed for the HADES experiment was chosen as front-end electronics for the TOF700. Signals from the MRPC are sent to the FEE over 50 ohm coaxial cables with MMCX connectors. The boards are based on the NINO ASICs, which, as already mentioned, process the signals in such a way that the duration of the LVDS output signals is proportional to the amplitude of the input signals, suitable for implementation of the time-over-threshold method. The output signals are transmitted to the digitizing module using DHR-78F connectors. A 64-channel VME TDC64VHLE time-to-digital converter based on the HPTDC chip is used for digitization. With a special module (PWR&CTRL) it is possible to remotely control the power supply, the discrimination threshold and hysteresis value in the FEE boards.

Prototypes of "cold" and "warm" TOF700 detectors were tested in the secondary muon beam of the U-70 accelerator at IHEP (Protvino, Russia). The test was carried out at the "MUON" facility with a particle flux of about 1 kHz/cm^2. A fast scintillation counter with its own time resolution of 40 ps was used as a start counter. The test results of both prototypes are shown in the figure 32. The intrinsic time resolution of the MRPCs with electronics is better than 45 ps with an efficiency of 98% and 95% for "cold" and "warm" chambers respectively.

Main parameters of the TOF400 and TOF700 sub-systems are summarized in Table 5.

8.3 Services system

Both TOF400 and TOF700 systems use the same a non-flammable Freon rich gas mixture containing 90% C2H2F4 + 5% i-C4H10 + 5% SF6. A simple open-loop gas system was designed for the BM@N experiment. This system is based on the MKS 1479A controllers for measuring and adjusting the absolute flow of components with an accuracy of 0.3%. The flow rate of the gas mixture can be adjusted in the range from 6 l/h to 90 l/h, but the typical value is 21 l/h, which corresponds to the exchange of 2 volumes per day. Also, one additional channel is available to

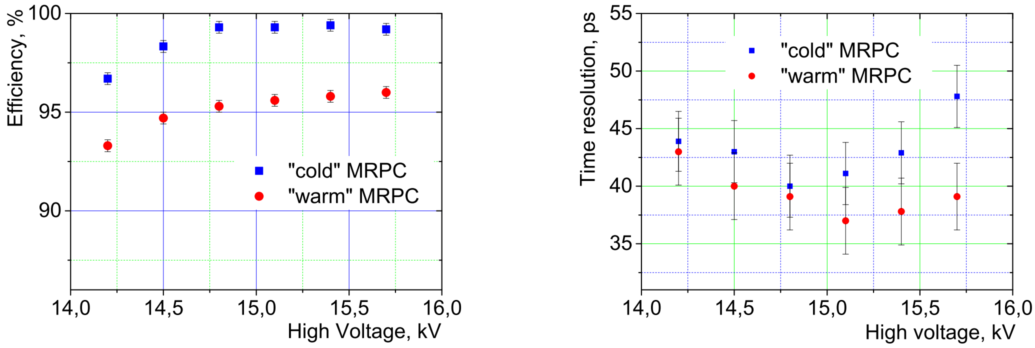

(a) (b)

Figure 32: Performance of the MRPC designed for TOF700 system. The detectors efficiency is shown on the left and time resolution on the right.

	TOF400	TOF700
MRPC active area	30x60 cm^2	30.3x56 cm^2 "cold" 16x35.1 cm^2 "warm"
FEE on one MRPC	96	32 for "cold" 64 for "warm"
Number of MRPC	20	30 "cold" 40 "warm"
Total active area	2 Arms x 1.1x1.3 m^2	3.2x2.2 m^2
Total number of FEE	1920	3520

Table 5: Main parameters of TOF system.

purge the system with nitrogen for cleaning and drying. A special PC program has been written to control the parameters of the gas system via the Ethernet interface.

The MRPC detector operates at very high voltage of 12 kV and 15 kV for TOF400 and TOF700 respectively. On the other hand, the dark currents of the detector are quite small at the level of tens of nA. Also, the detector is very sensitive to voltage ripples due to the large capacitive coupling between the high-voltage layer and the readout strips. Therefore, the high-voltage system is subject to high requirements for voltage stability and current measurement accuracy. The high-voltage power supply systems for both TOF sub-systems are based on commercially available ISeg modules and a specially designed HVSys power supply. Remote control of all elements of the system is organized via Ethernet interface.

To monitor stability of operation of the TOF sub-systems, controlled parameters are sent to the Slow Control System. The data are displayed on the website of the experiment via Grafana. The operator can see the value of the applied high voltage and measured current in the detectors, the thresholds of the amplifiers, the gas flow and the weight of the gas in cylinders, and some other parameters. In case of a malfunction, the operator receives a warning message that allows to respond in time. All monitored parameters are stored in a database and can be used in the offline analysis.

9 Outer tracker

The purpose of the outer tracker is to provide link between tracks measured in the central tracker and hits in the ToF-400 and ToF-700 detectors. In the Run 8 outer tracker consisted of two large aperture drift chambers (DCH), four CSC (cathode strip chamber) with the size of the active area of 1129×1065 mm^2 and one plane of 2190×1453 mm^2 CSC (see Fig. 1).

9.1 DCH

The drift chambers [16] have an octagonal shape with a transverse width of 2.9 m. (Fig. 33).

Figure 33: DCH integrated into BM@N experimental setup.

Their fiducial area is about 4.5 m^2. Every drift chamber (DCH) consists of 4 double coordinate planes with the following parameters: the wire inclination angles of 0^o, 90^o, $\pm 45^o$, the wire pitch of 10 mm, the outer dimentions of the sensitive area of Yout ± 1.2 m, Xout ± 1.2 m, the beam hole radius of R = 160 mm, 256 wires per coordinate plane, 2048 wires per chamber.

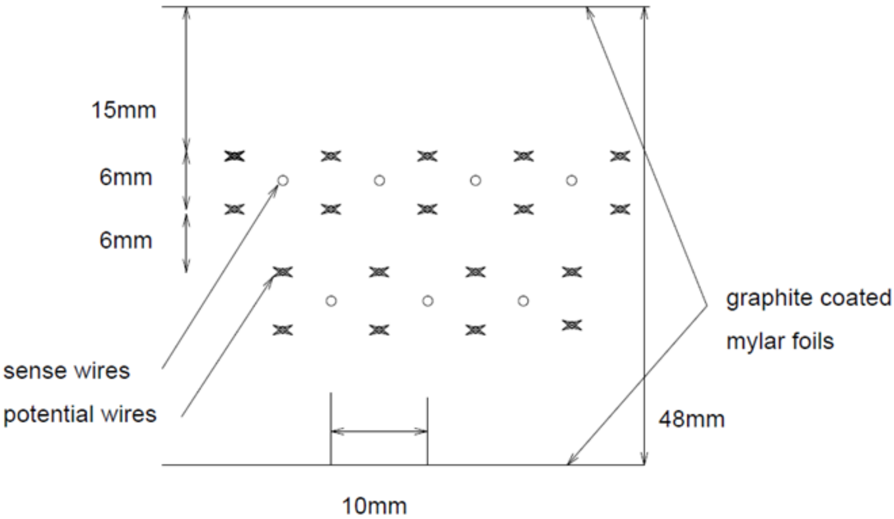

Figure 34: Drift cell geometry of the DCH.

To minimize multiple scattering effects, the wire chambers are constructed with minimal amount of material along the beam direction. A schematic view of the geometry of one view is shown in Fig.34. Sense wires have a diameter of 20 μm and made of gold-plated tungsten. The electric field is created by applying a negative voltage on two planes of gold-plated Ti-Cu wires located on each side of the sense wire planes, at a distance of 3 mm. The field wires have a diameter of 120 μm. The spacing between sense and field wires on a plane is 10 mm. Thin Mylar foils (22 μm) coated with graphite are used to shape the electric field in the drift cell and also to act as separating walls between two consecutive views.

A readout time measurement accuracy of about 1 ns with no deadtime is achievable with specially designed amplifiers and TDC circuits [17]. The anode signals in the wire chambers are amplified, discriminated and transformed to logic pulses in electronic circuits located on the chambers. The output pulse is a logic 50 ns wide ECL pulse with 50 ns deadtime following the pulse, achieved by a delay element.

The granularity of DCH is sufficient to perform measurements of interactions with light ions (up to Ar). The DCH wire occupancy in interactions of middle and heavy nuclei is too high to perform efficient track separation. Thus, the DCH will be replaced by cathode strip chambers (CSC) to perform track measurements in middle and heavy nucleus collisions.

9.2 CSC

The full configuration of the outer tracking system for heavy ion program will consist of four planes of 1129×1065 mm^2 CSC (cathode strip chamber) and two planes of 2190×1453 mm^2 CSC. The CSC detectors are situated outside the magnetic field with the aim to make precise link to the tracks, reconstructed in the GEM detectors inside the analyzing magnet. Tracks refined in CSC are used to improve particles momentum reconstruction and to find corresponding hits in the time-of-flight systems ToF400 and ToF700.

The first CSC detector with the size of the active area of 1129×1065 mm^2 was designed and assembled at LHEP JINR in 2018. It consists of an anode plane located between two cathode planes (see Fig. 35). The anode plane is a set of gilded tungsten wires with the diameter of 30 μm which are fixed on the plane with a step of 2.5 mm. The gap between the anode plane and each cathode plane is 3.8 mm. Two-coordinate readout of the signal is performed on two cathode PCB boards using sets of parallel metal strips. The inclination angles of the cathode strips to the vertical axis are 0 degrees (X coordinate) and 15 degrees (Y coordinate). The pitch of the X and Y strips is 2.5 mm. PCBs are glued to the support honeycomb. Due to a large multiplicity of charged particles in Au-Au collisions, readout layer is divided into outer (cold) and inner (hot) zones.

First beam tests of the 1129×1065 mm^2 CSC were performed in 2018 at the argon beam with kinetic energy of 3.2 AGeV and the krypton beam with kinetic energy of 2.3 AGeV at the Nuclotron. The CSC was installed upstream the ToF-400 time-of-flight detectors. The main goal of the tests was to study the performance of the CSC detector and the FEE and readout electronics as a part of the BM@N experimental setup. The signal clusters were reconstructed as groups of adjacent strips with amplitudes of signals above the threshold. For the reconstructed clusters, the center of gravity, the width and the total charge were calculated. The average cluster width is 6 strips which is equal to 15 mm. The gap size between the anode and cathode is reduced to 3 mm instead of 3.8 mm in order to improve the spatial resolution in multitrack events.

All four CSC detectors with the size of the active area of 1129×1065 mm^2 and one detector CSC with the size of 2190×1453 mm^2 were integrated into the BM@N setup in the physical run 2022-2023 with the Xenon beam at the kinetic energy of 3.8 AGeV at the Nuclotron

Two CSCs of the size 2190×1453 mm^2 have been designed to cover the ToF-700 system on both sides and replace the existing drift chambers (DCH). The design of these cathode strip chambers is shown in Fig. 36. One cathode plane consists of 8 PCBs, each PCB is divided into hot and cold zones. The hole in the center of the chamber is designed for the vacuum beam pipe. The gap size between the anode and cathodes is planned to be 3 mm. Two-coordinate readout of the signal is performed using sets of parallel metal strips with the inclination angle of 0 degrees for the X coordinate and 15 degrees for the Y coordinate. The pitch of the X and Y strips is 2.5 mm.

9.2.1 Front-end electronics

Front-end electronics is based on the same charge sensitive pre-amplifier chip VA163 as used for the GEM detectors. The multiplexed data from each board are transmitted through the twisted pair

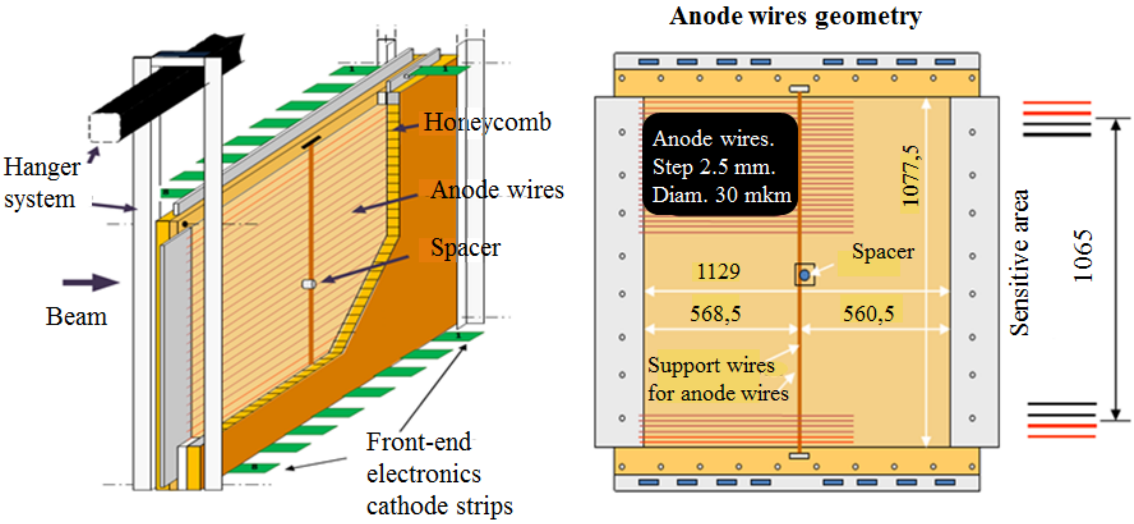

Figure 35: Schematic view of the 1129×1065 mm^2 CSC

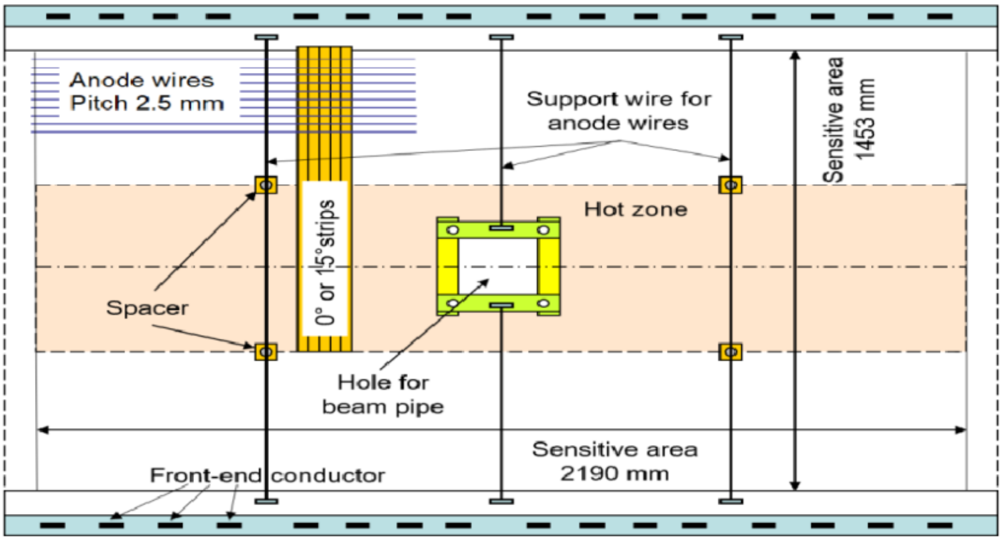

Figure 36: A technical drawing of the cathode strip chamber of the size 2190×1453 mm^2 (15-degree strips are not shown in this picture).

flat cable to the 12-bit analog-to-digital converter (ADC) readout by the BM@N data acquisition system.

The full configuration with 6 CSC detectors equipped with the electronics based on VA-163 chips (35000 readout channels) is planned to be integrated into the BM@N experimental setup at the 2023.

9.2.2 Gas distribution system

The outer tracker were operated with Ar(75%) + C_4H_{10}(25%) / C_3H_8O (vapor) gas mixtures. The gas system (Fig. 37) consists of two parts: 1) the mixer system which delivers a mixture of gases in a required ratio and pressure to downstream elements; 2) the distribution system, which delivers the gas in well defined quantities to the individual detectors.

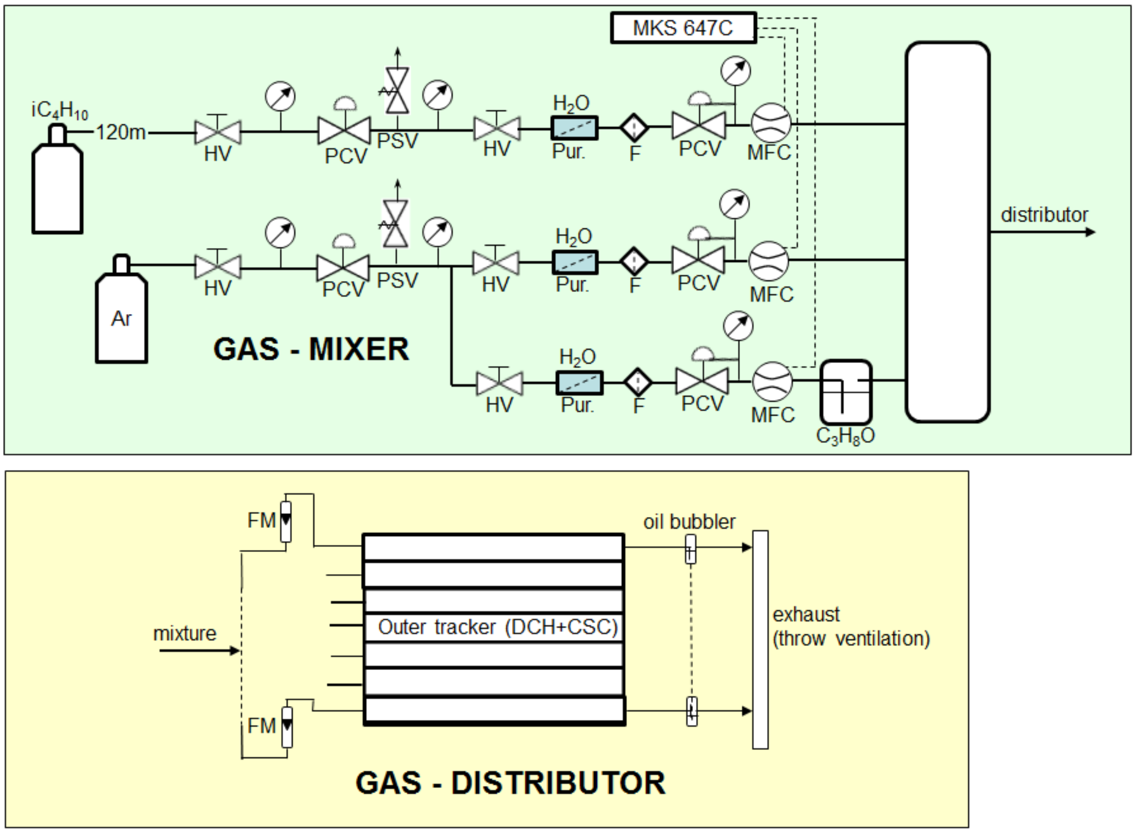

Figure 37: The gas line for the outer tracker. The layout of the mixer module: HV – on/off valve, PCV – pressure control (constant) valve, PSV – pressure safety valve, Pur. – Purifier (H2O and O2), F – filter, MFC – mass flow controller (MKS Instruments firm), MKS 647C – power supply and readout (MKS Instruments firm). Component layout of the distributor module: FM – flowmeter (manually flow adjustment), oil bubbler – pressure and air protection.

10 Forward Spectator Detectors

The new forward detectors for measuring the energy (FHCal) and charges (FQH, ScWall) of projectile spectators produced in the nucleus-nucleus collisions in the BM@N experiments have been developed and constructed during last few years. They are located at the very end of the BM@N facility. These detectors are used to determine the centrality and orientation of the reaction plane. Moreover, ScWall and FQH can be used also to study the charge distributions of spectator fragments produced in the nucleus-nucleus interactions.

10.1 Forward Hadron Calorimeter (FHCal)

The forward hadron calorimeter FHCal has a granular structure in the transverse and longitudinal planes. It consists of 54 separate modules which provides transverse granularity of the FHCal. Internal part of the FHCal consists of 34 small modules with transverse sizes of $15\times15\text{cm}^2$ and a length equivalent to 4.0 nuclear interaction lengths. These modules are identical to the modules of the forward hadron calorimeters of the Multi-Purpose Detector (MPD) experiment at the NICA accelerator complex [8]. Two outer lateral parts of the calorimeter consist of 10 large modules on each side with transverse sizes of $20\times20\text{cm}^2$ and a length equivalent to 5.6 nuclear interaction lengths. These modules were initially constructed for the hadron calorimeter of the Compressed Baryonic Matter (CBM) experiment (FAIR, Darmstadt, Germany) [9] and are temporarily used in the hadron calorimeter of the BM@N experiment. Schematic view of the FHCal is shown in Fig. 38, left. At the center of the calorimeter there is a hole with transverse size $15\times15\text{cm}^2$. Noninteracted beam ions pass to a beam dump located behind the calorimeter through this hole. It is necessary to protect internal modules of the calorimeter against high radiation dose and strong activation in experiments with heavy ion beams.

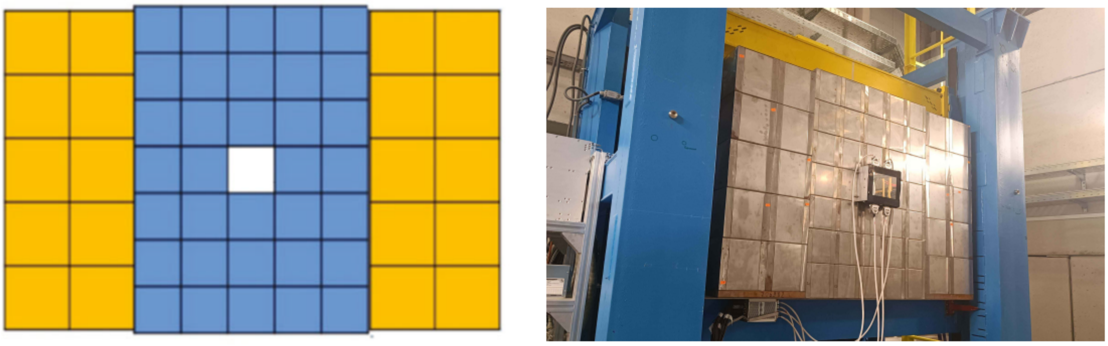

Figure 38: Schematic view of the FHCal, left. Photo of the FHCal with FQH installed on the the movable platform (blue) at the BM@N, right.

FHCal modules have sampling structure and consist of lead/scintillator layers with a sampling ratio of 4:1 (the thickness of the lead plates and scintillator tiles are 16 mm and 4 mm, respectively) and provide compensation condition (e/h=1) for the hadron calorimeter. Small modules have 42 lead/scintillator layers and large modules have 60 such layers. To get rather hard rigidity of the lead plates they are made of lead-antimony alloy. An assembly of 60 (42) alternating layers of scintillator and lead plates are tightened into one package with a 0.5 mm thick stainless steel band using a special tensioning mechanism. The tape is welded with spot welding to the steel plates inserts installed in the beginning, middle and end of the package (Fig. 39). Behind the tightening mechanism the block of boron polystyrene with thickness 10 cm is installed in large modules. Once the package is assembled, it is closed by an upper box of 0.5 mm thick stainless steel sheet.

The scintillator plates are made from polystyrene-based plastic scintillators produced by Uniplast (Vladimir, Russia). Light from each scintillator plate is collected by wavelength shifting optical fiber KURARAY Y-11(200) glued into groove with depth 1.2 mm on the surface of the scintillation plate and transported to the end of module. The grooves in scintillators of large modules have circular form, while grooves in scintillators in small modules are spiral. Outside of the scintillator plate fibers are placed in thin black plastic pipes to be optically shielded and are stacked in parallel on the top surface of the module package. All scintillators with glued fibers are wrapped in Tyvek reflector.

The end of each fiber glued in the scintillator plate is coated with reflective paint. At the end of the module the optical fibers from each of the six consecutive scintillation plates in the module are glued into individual optical connectors, which are placed on a panel mounted in the module box. Thus, each of large modules has ten longitudinal sections and each of small modules has seven sections. The longitudinal segmentation provides high homogeneity of light collection along modules, a large dynamic range of the calorimeter response and makes it possible to perform energy calibration of FHCal with cosmic muons [10].

This panel with ten optical connectors for large module (seven optical connectors for small module) has an additional optical connector for LED light distribution system. LED pulses are distributed with ten (seven) optical fibers into each section optical connector. Light pulses from the LED allow to control the operation of the photodetectors used for light readout.

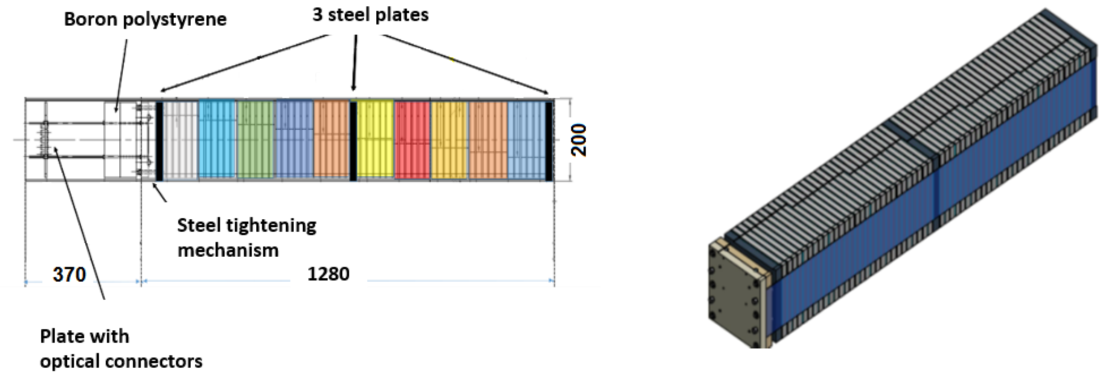

Figure 39: Left - scheme of large module, here 10 sections are shown in different colors. Right - 3D view of the large calorimeter module in assembly.

The weight of each small module is about 200 kg and weight of large module is about 500 kg. Total weight of the FHCal is about 17 tons. It is mounted on the special platform shown in blue color on Fig. 38, right, which is able to move FHCal in X-Y directions.

10.1.1 FHCal photodetectors, FEE and readout electronics

The Hamamatsu MPPC S12572-010P with $3{\times}3\text{mm}^2$ sensitive area are used as photodetectors for light detection from the sections of the FHCal. These photodetectors have gain $1.35{\times}10^5$ and photon detection efficiency about 10% at peak sensitivity wavelength 470 nm. Due to very small pixel pitch - 10mkm - the total number of pixels is 90000 which is important to provide the linear response in wide dynamic range of the signal. FHCal Front-end-electronics (FEE) is composed of two separate PCBs. Ten (seven) photodetectors are installed on a first PCB directly connected with light connectors at the end of each large (small) module. A temperature sensor is mounted near photodetectors on aluminum heat sink. The second PCB contains signal preamplifiers with differential ADC driver output and individually adjustable voltage regulation circuits for the photodetectors. This board has also LED flash generation circuit with synchronization input and analog sum signal output. All FEE boards are remotely controlled via specially designed HVSys System Module manufactured in JINR (Dubna, Russia).

There are 438 calorimeter sections, which are needed to be readout. Eight ADC64s2 boards, produced at JINR (Dubna, Russia) are used for signal readout. They have 64 channel 12-bit ADCs with sampling rate of 62.5 MHz and memory depth of up to 1024 points per channel. The ADC64s2 boards have Lemo connectors for trigger and Xoff signals, and are capable of time synchronization via White Rabbit network, providing per-channel zero suppression function with adjustable threshold and can operate in self-triggered or externally triggered modes. FHCal ADCs are fully integrated into the BM@N data acquisition system which provides trigger signals, busy logic, White Rabbit network and data readout. Power for FHCal ADCs is provided by a remotely controlled power supply units placed in Wiener crate.

Custom 12-channel analog sum modules (adders) with individually adjustable attenuation have been constructed. These adders are used to sum up the analog outputs from FHCal modules. They are used when performing standalone cosmic calibrations in central DAQ. The adders can be used for integration into the BM@N trigger system.

10.1.2 FHCal calibration with cosmic muons, energy resolution and linearity of the response

Since muon beams are unavailable at the BM@N setup, energy calibration of the FHCal can only be performed using cosmic particles. Longitudinal and transverse segmentation of the calorimeter allows for track reconstruction [10], which was used to compensate for track length variation in the scintillator tiles due to varying track orientation of the cosmic particles. Cosmic calibrations parameters show 40 - 50 photoelectrons per one muon per one section.

A detailed study of the linearity of response and energy resolution for array of 9 large modules has been performed on protons with kinetic energy range 1 - 9 GeV at the CERN T9 and T10 beamlines [11]. The good linearity and 0.54/sqrt(E) energy resolution was obtained.

10.2 Forward Quartz Hodoscope (FQH)

The FHCal beam hole is covered with beam hodoscope - Forward Quartz Hodoscope (FQH). The main goal of the FQH is measuring charges of spectator fragments which pass the beam hole of the calorimeter in order to estimate the collision centrality with combined FHCal and hodoscope response. The FQH consists of 16 strips - cherenkov detectors - with sizes of $16 \times 1 \times 0.4\text{cm}^3$ (see Fig. 40, left) inside light tight box. Each FQH detector has light readout with two individual silicon photo-multipliers mounted on opposite sides of the strip (see Fig. 40, right).

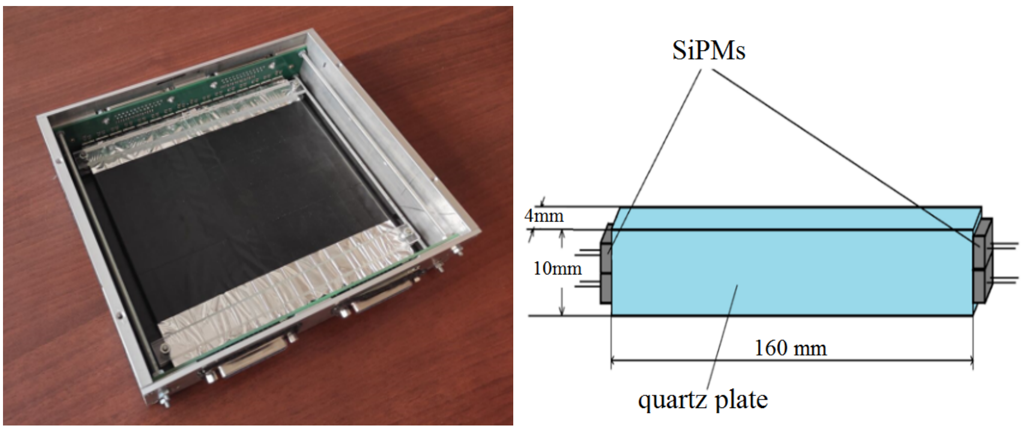

Figure 40: Left: photo of Forward Quartz Hodoscope - FQH (inside view). Right: picture of the FQH strip with SiPM photodetectors mounted.

One Front-End-Electronic (FEE) board reads eight channels. Total number of FEEs are four for full FQH. The FQH installed in front of the beam hole of FHCal is shown in Fig. 38 (right). Four FEE boards of FQH are connected to the control box with amplifiers installed at bottom side of FHCal.

Hamamatsu MPPCs S14160-3015PS with 3x3 mm2 sensitive area and PDE of 32% are used as photodetectors. Four TQDC-16 boards with total 64 channels are used to read-out the two-gain outputs from each photodetector. The gains are 1x and 4x. Low gain channel is used for maximum dynamic range up to the highest ion charge expected. High gain channel is used for low-Z fragments. Charge calibration of FQH strips is performed with pure beam ions.

10.3 Scintillation Wall (ScWall)

The ScWall is the large area detector aimed for measuring the charged particles in forward rapidity. It consists of array of scintillating plates placed in the aluminum box. The view of the ScWall is shown in Fig. 41. The full detector size is $270 \times 130\text{cm}^2$. The ScWall has 40 inner small ($7.5 \times 7.5 \times 1\text{cm}^3$) scintillator detectors (cells) and 138 big outer cells ($15 \times 15 \times 1\text{cm}^3$). In order to avoid heavy-ion beam radiation damage the very central part of ScWall has $15 \times 15\text{cm}^2$ beam hole (see Fig. 41). The cells are made of polistirol-based scintillators are manufactured at "Uniplast" (Vladimir, Russia).

The light in the cells is collected by WLS Y11(200) S-type (Kuraray) fibers mounted in 1.5mm deep grooves (see Fig. 42) and detected by SiPM Hamamatsu S13360-1325CS with $1.3 \times 1.3\text{mm}^2$ active area, gain of 7×10^5 and PDE of 25%. The measured light yields of big cells and small cells are about 32 p.e./MIP and about 55 p.e./MIP, respectively. The full area of ScWall is divided into 12 read-out zones and performed with ADC64s2 board combined with FEE boards. Three

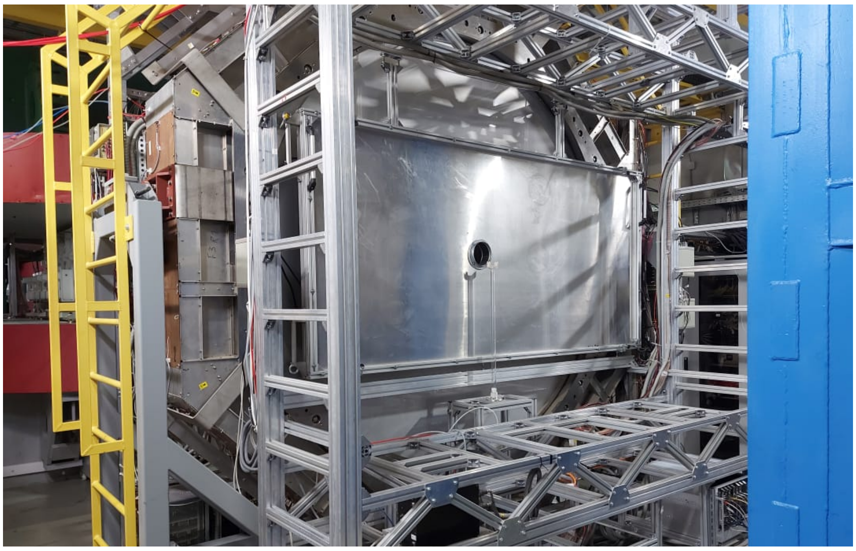

Figure 41: The view of ScWall detector with the beam hole.

ADC64s2+FEE boxes are used for read full ScWall. The calibration of ScWall cells has been performed on cosmic muons as well as on Z=1 charge particles coming from the ion-ion reaction.

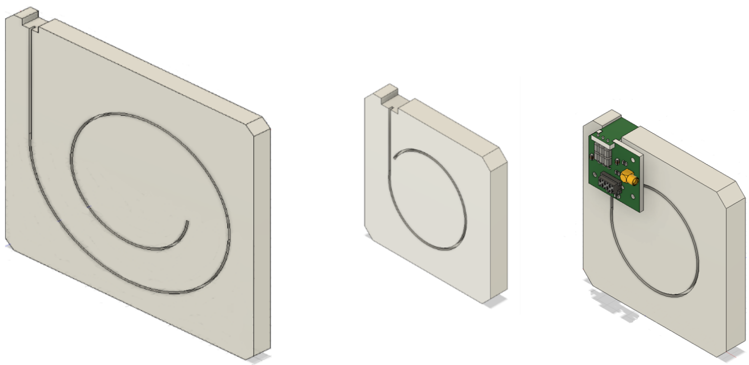

Figure 42: From the left to the right: schematic view of large ScWall cell, schematic view of small ScWall cell, schematic view of small cell assembly with SiPM on PCB board with connectors.

10.4 Slow Control for forward detectors

The FHCal, FQH and ScWall have SiPMs as light detectors. In order to control and monitor bias voltage (HV) applied to SiPMs and the temperature the new Slow Control system has been developed. The hardware part of Slow Control is designed and constructed by "HVsys" (JINR, Dubna). HV power supply modules have multi-channel HV supplies with micro-controller interface. Schematic view of Slow Control system is shown in Fig. 43. Each HVsys system module has a unique IP-address for communication through individual proxy-server. Communication of HVsys box with FEE micro-controllers is done with RS-485 interface. All proxy-servers have connections to GUI panel to control and monitor status and to perform temperature correction for all SiPMs. The software part of the Slow Control is written on python3 [12].

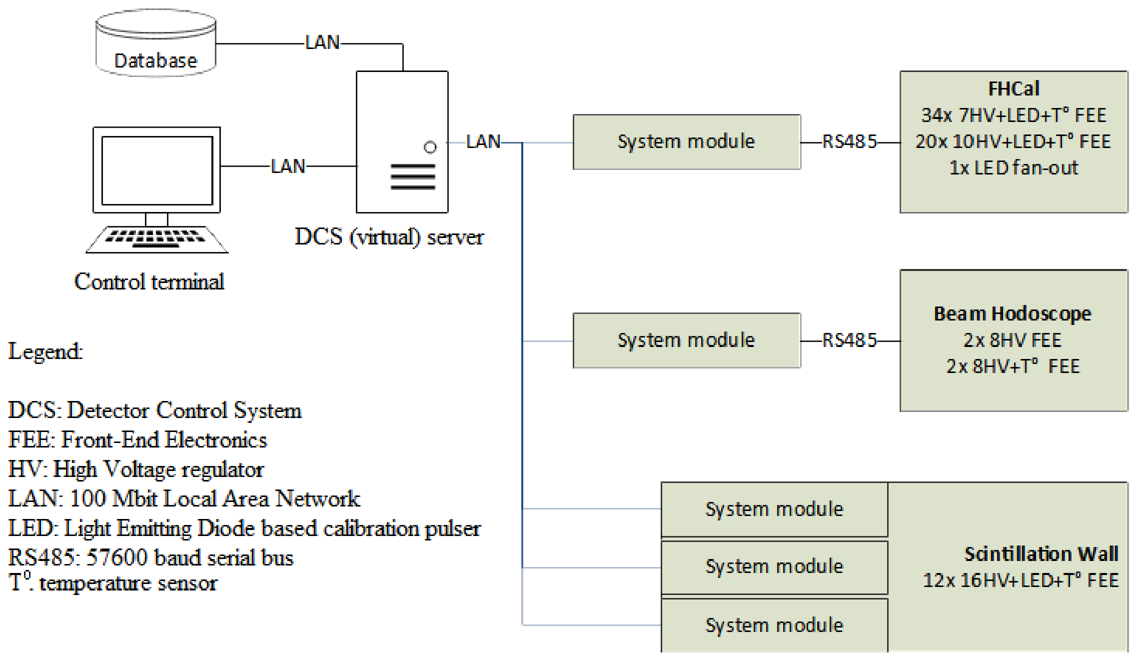

Figure 43: The Slow Control system for forward detectors at BM@N.

11 Trigger

BM@N trigger consists of hardware and sofware parts. The hardware part includes detectors on fast plastic scintillators, low- and high- voltage power suppliers, programmable trigger logic unit T0U, trigger control unit CAEN N6742. The software part include a graphic trigger interface, trigger performance and beam quality control.

A beam trigger BT formed by the signal coincidence from beam couters BC1, BC2 under condition the signal absence from the veto counter VC:

$$BT = BC1 \times BC2 \times VC(veto)$$

A minimum bias trigger MBT asks only for a low amplitude signals in forward counter FD, which corresponds to the beam particle interaction in a space between BC2 and FD counters:

$$MBT = BT \times FD(veto)$$

The interaction trigger called Central Collision Trigger (CCT) composed of the minimum bias trigger and the multiplicity in the barrel detector:

$$CCT = MBT \times BD(> N)$$

All the triggers mentioned above (BT, MBT, CCT) are send in the output data stream with the corresponding scaling factor.

Trigger decision formed by the programmable logic controller T0U and its logic organisation is shown in Fig. 44.

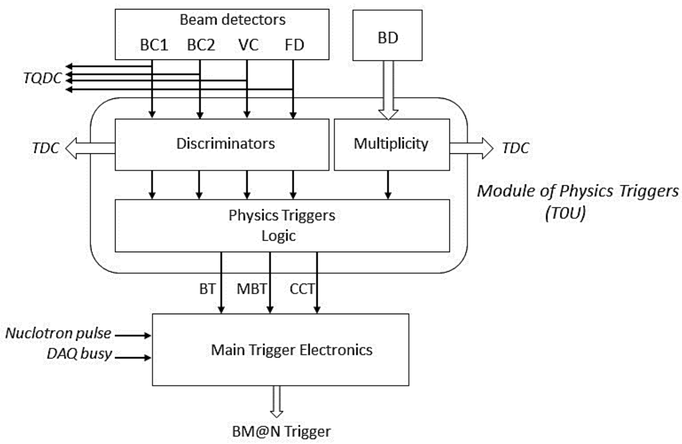

Figure 44: Trigger logic.

12 BM@N DAQ: Hardware Architecture

The core function of the DAQ system is realization of data transfer from the detector to the storage system. It includes the data flow from readout electronics to the First Level Processor (FLP) fabric, to the Event Building (EB) and to the Storage System. Main DAQ components are readout electronics modules, clock and time synchronization system, trigger distribution system, data transfer networks, data processing servers and online storage system ($\_link - to - tdr\_$). The general architecture is sketched in Fig. 45.

Detector Readout Electronics (DRE) boards record detector signals. There are two main types of DRE boards grouped by function: Timestamping Time to Digital Converters (TDC), Waveform Digitizers or Amplitude to Digital Converters (ADC).

12.1 TDC DRE board

TDC DRE board performs time-stamping of discrete signals (hits) with typical accuracy of $20ps$. It is based on HPTDC chip. Hit timestamps are kept for $51\mu s$ in ring type memory. The total trigger latency should not exceed this value. ADC DRE board is a waveform digitizer. It quantize analogue input signal and samples it at fixed time intervals. Zero suppression logic is based on baseline estimation and threshold value. Signal shaping can be performed in digital form with FIR filters. It allows to reduce the number of waveform points required for digital signal representation with minimum loss of accuracy. The ring type memory allows the read back of last $32\mu s$ of waveforms. It sets the limit on trigger latency to this value. TQDC DRE board combines both TDC and ADC functions.

12.2 MSC16VE module

MSC16VE is 16-channel multievent scaler (Fig. 47). Each channel input has 50Ω impedance and accept signals of ± 2.5V range and discrimination threshold can be adjusted in $\pm$ 1V range. Module has 4 LVTTL count enable (CE) inputs. Ethernet 1000BASE-X connection is used for data readout and module control. Module MSC16VE has three main logic parts: input part, multi-event data readout and hardware histograms. Input part has crosspoint switch that allows any input channel to be processed by any multi-event counter and histogram. CE and Gate logics have 16 independent Look-Up Tables (LUT) each. Gate logic determines reset conditions for hardware histograms. Multi-event counters data continuously splits into numbered time slices and pushes to data encoder and further to Ethernet. Time slices length is adjustable with minimum length of 64 ns and 8 ns step. Data encoder perform zero suppression and data packing. Hardware histograms are used for online monitoring of input hits. Time series histograms store hits distribution in time. Time interval histograms store time interval between two adjacent hits in channel. Both hardware histograms readout by request from control software.

12.3 Timing System

White Rabbit provides sub-nanosecond accuracy and picosecond precision of time synchronization for distributed systems. DRE boards digitize detector signals using common notion of time and frequency provided by the White Rabbit (WR) network. The time reference is provided by GPS/GLONASS receiver and backup precision frequency reference (Rubidium clock). Digitizer boards require precise reference clock for high precision measurements. Timestamping TDCs used in T0, TOF400, TOF700 detector electronics have time resolution of $25ps$, DCH-$100ps$. DRE boards include White Rabbit Node Core and tunable crystal oscillators that are synchronized to reference clock with $10ps$ accuracy. WR node core provides local clock and timestamp at 125 MHz. The timestamp is specified as TAI (International Atomic Time). It is an absolute number of seconds and nanoseconds since 01.01.1970. Frequency dividers synchronized by 1 PPS (Pulse per Second) signal are used to produce digitizer clocks: 41.667 MHz for HPTDC ASICs and 62.5 MHz for waveform digitizers.

12.4 Trigger distribution system

BM@N trigger system has tree structure and 3 trigger levels: L0, L1 and L2.

12.4.1 General architecture of trigger distribution system

L0 is fast trigger signal for front-end electronics with latency of $150ns$. L1 trigger signal is readout trigger candidate generated by TRC module (see 12.4.2), according to its internal logic. Formation time of L1 trigger is adjustable and was $\tilde{1}\mu s$ in BM@N run 8. L2 trigger, produced by UT24VE module (see 12.4.3), starts data readout for all subsystems. All signals are transmitted via coaxial cables in LVTTL standard. Trigger-Busy handshake algorithm for L2 trigger was implemented to guaranty all triggers delivery to all subsystem. This algorithm is shown in the Fig. 48. Rising edge of trigger signal (1) leads to rising edge of busy signal (2). After that trigger signal is deasserted (3). Upon completion of data collection, the subsystems deassert busy signals (4). Typical subsystems busy time shown in the Fig. 49.

12.4.2 TRC – Trigger Control

TRC (TRigger Control) module was designed for BM@N run 8. Main goal of this module is production of readout trigger candidates (L1) according to its configurable logic. T0 unit is used as source for input signals ("physical" triggers BT, CCT, MBT, etc.). Each of 16 input channels has individual settings: input delay, hits downscaling factor and before/after protection. Before/after protection logic used for pile-up rejection and secondary hits rejection during detectors dead time. L1 trigger candidate output delay can be adjusted in range of 8 ns to 100 μs. TRC module produces L0 trigger for GEM, CSC, FSD and BT front end electronics, as they required fast (less then 300 ns) data latch signal. Different conditional counters for input physical triggers are implemented in TRC module.

12.4.3 LTU - Logical Trigger Unit

LTU is main module for L2 trigger generation and distribution system. The module ensures the operation of Trigger-Busy handshake algorithm (Fig. 48) and can process up to 16 busy channels. Busy signals can be received from DRE modules or hierarchically lower LTU modules. Time intervals between accepted triggers and busy signals duration are histogramed in LTU internal memory. Various trigger counters are also implemented in module.

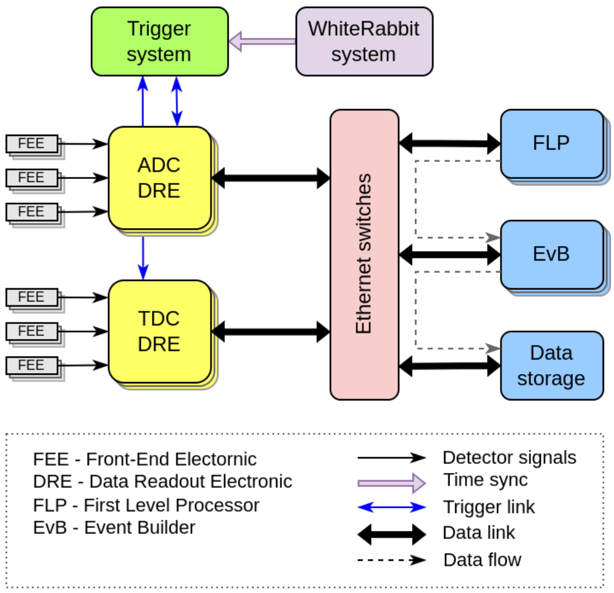

Figure 45: General architecture of DAQ system

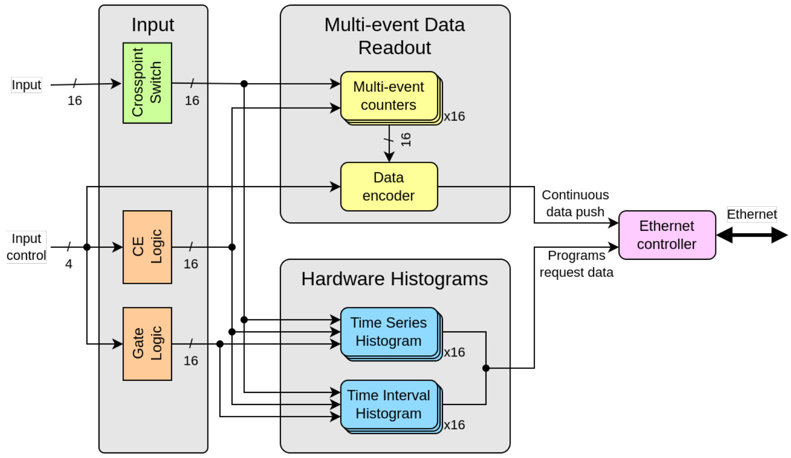

Figure 46: MSC16VE module.

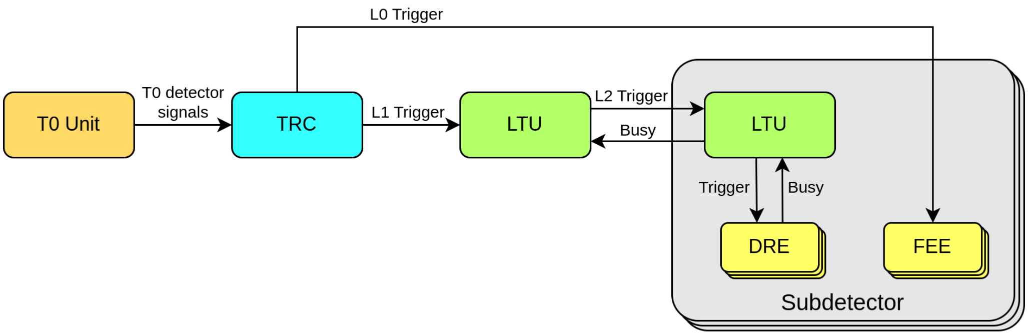

Figure 47: BM@N trigger architecture.

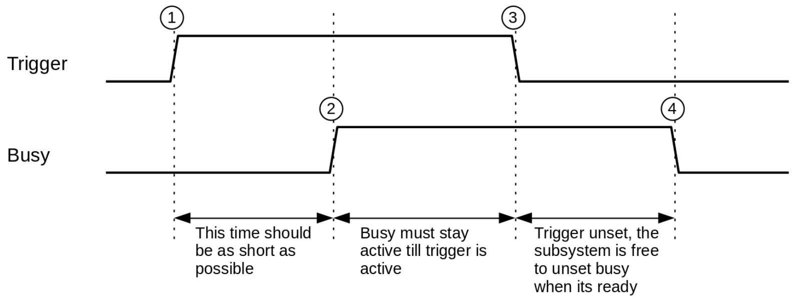

Figure 48: Trigger handshake chronogram.

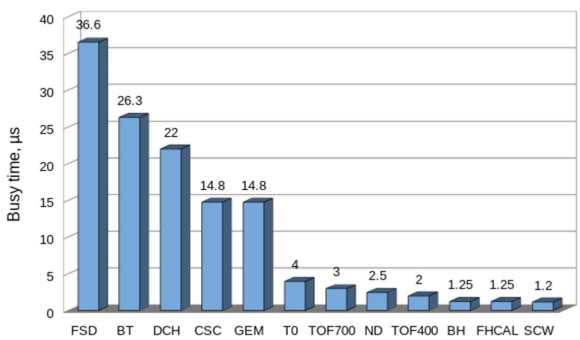

Figure 49: The average busy time for all subsystems.

12.5 DAQ data flow

All BM@N subdetectors except DCH use Ethernet to transfer data from readout electronics to First Level Processors. Primary FLP task is to receive data stream in real time, buffer, validate, format and enqueue data blocks to event building network. FLP decouples fast microsecond-scale synchronous data acquisition process from slower seconds-scale software data processing by buffering data in computer RAM. Data transfer path from readout electronic module to event building network and storage system is shown on Fig. 50 for typical 64-channel ADC based waveform digitizer module ADC64VE.

Electronic modules designed by DAQ team share common communication architecture. Network connectivity is provided by hardware IP stack (HWIP), a programmable logic code synthesized for onboard FPGA processor. Taking into account limited memory and logic resources of FPGA chips available, and implementation complexity of TCP protocol, custom data transfer protocol MStream has been designed for data streaming over 1 Gb/s or 10 Gb/s Ethernet networks. It uses UDP over IP as transport layer, and implements ordered and reliable data packet delivery using acknowledgments.

FLP receive data stream in real time. Dedicated servers with dual 18-core CPUs, equipped with dual 100 Gb/s Ethernet adaptors, are running Fedora-36 Linux OS. Tuning for real-time operation is necessary to ensure continuous data transferred without interruptions [18]. It includes CPU frequency and supply voltage management, network adapter interrupt coalescence mitigation and system task scheduler adjustments.

BM@N readout electronics deliver 6 GB/s of raw data over 200 streams in peak at 10 kHz trigger rate. Single data stream has 500 MB/s maximum sustained throughput when using 10 Gb/s Ethernet. Run 8 operation has shown that single manually tuned FLP server is capable of hosting 10-12 data stream receivers with minimal contribution to overall busy time.

Software event building in BM@N is part of asynchronous processing, it does not affect readout busy time under normal operation. Event builders are cascaded in multiple layers for load distribution, and last layer writes data files to storage system.

Event Builder programs associated with data intensive subdetectors run on dedicated hardware servers, while event builders for low data rate subdetectors run in KVM virtual environment, as well as readout control programs. It allows to utilise computer resources efficiently.

12.6 DAQ storage system

DAQ storage system is comprised of 10 servers with NVMe solid state devices for low latency I/O operations and 12 servers with hard disks for high volume storage. It is distributed software defined object storage cluster under control of Ceph software ([19]). Cluster management and interface functions are implemented on 6 dedicated single-CPU servers. Configurable 'CRUSH map' algorithm defines data object to storage device mapping. Ceph cluster has self recovery functions and it performs periodic data read check on regular intervals to ensure data integrity. It is highly available and reliable system with no single point of failure.

Storage devices are organised in pools with different data redundancy algorithms. Pools allocated on NVMe devices have triple replication provide 100 TB usable space, and are used as block storage for virtual machine cluster. Hard disk pool has 2.2 PB usable capacity. It use erasure coding replication with 40% overhead. POSIX compatible filesystem interface CephFS is used for experimental data storage. Server hardware characteristics are shown in Table 6.

Qty	Function	Specifications	Network
20	Compute node	Dual 18-core 3 GHz CPU, 384 GB RAM	Dual 100 Gb/s
10	NVMe storage server	$10 \times 3.5 TBNVMe$	Dual 100 Gb/s
8	HDD storage server 1	$24 \times 12TBHDD, 1.8TBSSDcache$	Dual 100 Gb/s
4	HDD storage server 2	$24 \times 18TBHDD, 3TBSSDcache$	Dual 100 Gb/s
6	Control server	4-core CPU, 64 GB RAM	Dual 25 Gb/s
1	Bootstrap server	4-core CPU, 16 GB RAM, $4 \times 300GBHDD$	Dual 1 Gb/s

Table 6: Characteristics of BMN DAQ server equipment.

12.7 Virtual computing cluster

Programs performing readout control functions, detector slow control, software and infrastructure monitoring and other services are run on KVM virtual machines or LXC containers that reside on highly available cluster. Approx. 100 virtual machines in total reside on 10 compute nodes. Cluster has backup and snapshot rollback mechanisms that are necessary for safe software administration and recovery in case of errors. Virtual cluster is also used as offline computing farm for batch and interactive analysis when no data taking is in progress.

12.8 BM@N DAQ IT Infrastructure

DAQ server equipment is located in 4 racks in MDC (modular data center), Fig. 52 49 servers occupy 81 units of rack space in total. Table ?? shows server types and functions.

Virtual machine cluster is comprised of 10 compute nodes running Proxmox VE version 7 software. Other 10 compute nodes are dedicated servers for FLP and event builders and run Fedora-36 OS. Storage servers run CentOS 8 Stream OS.

Basic network infrastructure services (RADIUS, DHCP, DNS) are provided by virtual cluster with redundancy. During cold startup, while virtual cluster is not yet ready, basic services are provided by bootstrap server. By design DAQ system is not dependant on any external network or software services and autonomous operation is possible.

Core of data network is two-level Ethernet fabric with Clos architecture that has two switches on spine level and multiple switches on leaf level Fig. 51. Ethernet VPN (EVPN) virtualisation technology is used to allow flexible traffic management, high availability and efficient link utilisation. Underlay network provide connectivity between fabric nodes, it is formed by leaf and spine switches connected with L3 routed links, topology is managed by OSPF dynamic routing protocol. Overlay network that carry user traffic is realised with MP-BGP protocol at control plane and VXLAN encapsulation at data plane.

DAQ network supports jumbo ethernet frames up to 9000 bytes to maximise throughput of data transfer from readout electronics. Network supports Any-Source Multicast that is necessary for automatic discovery of readout electronics modules and software components of distributed DAQ system.

Two spine and four leaf switches are located in racks of MDC. Other leaf switches and access switches of slow control systems are located in electronics racks in experimental area. Two core routers of DAQ technological network are located in building 201 and provide connectivity to campus network with 200 Gb/s bandwidth.

Compute and storage servers, readout electronics and additional level of 1 Gb/s access switches for slow control systems are connected to fabric leaf switches. Critical components have dual connections to pairs of leaf switches for high availability using LACP link aggregation protocol.

DAQ network has shown no critical problems during BMN data taking Run 8. Ethernet switching fabric bandwidth is adequate for peak traffic conditions and has no negative impact on data taking performance. No significant packet drops or errors were registered by monitoring system on network fabric switches that could indicate network saturation and packet buffer overflows. Considering both trigger rate and event size increase on next data taking run, it is possible to double fabric bandwidth by additional leaf to spine connections.

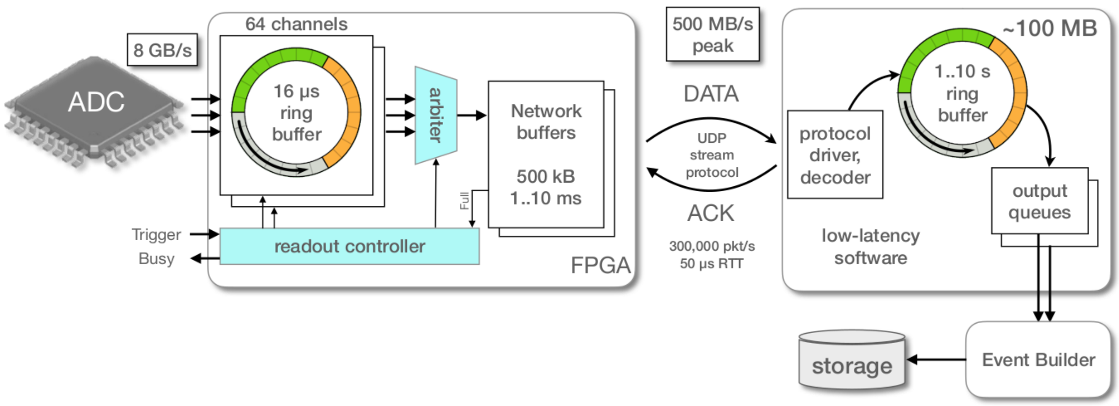

Figure 50: Data transfer from detector to storage system.

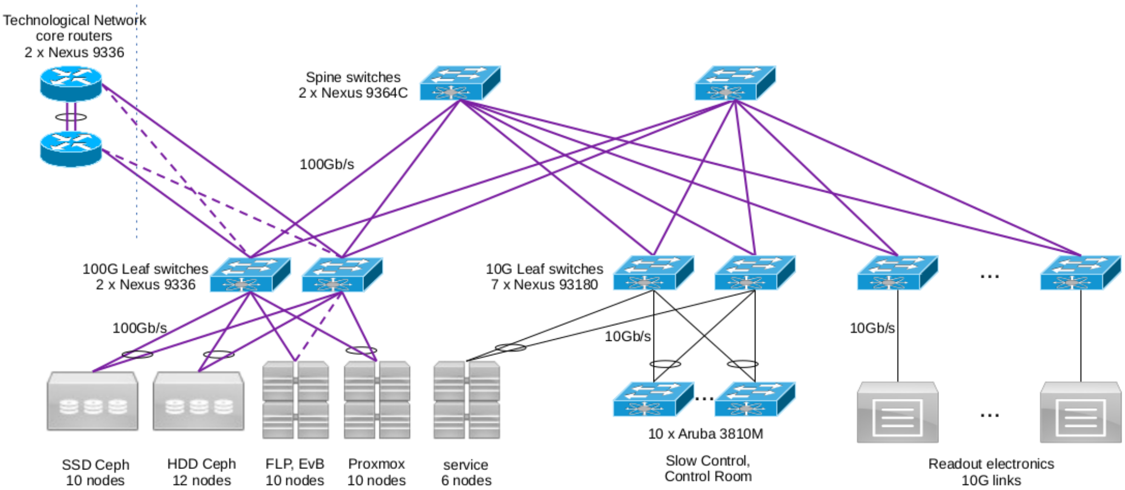

Figure 51: BMN DAQ Network.

Figure 52: BM@N Modular Data Center server racks.

13 Slow Control System

Main objectives of Slow Control System (SCS) include hardware status monitoring, archiving the operational properties of the facility, user-friendly graphical interface and alarm management system. The SCS was built around “TANGO Controls”[20] - an open-source toolkit, widely used in scientific experiments.

Slow Control data from experiment subdetectors such as: high voltage, low voltage, vacuum, gas flow and mixture etc. are aggregated by SCS. Those are then stored in the “historical database” - a PostgreSQL database with TimescaleDB extension[21]. It is implemented as distributed cluster with backup and load balancing

The user interface for live monitoring and retrieving past data is developed with Grafana[22] – an open-source analytics and interactive visualization web application. A mnemonic scheme of the experiment displaying hardware status and alarms (Fig. 53) was also implemented with it.

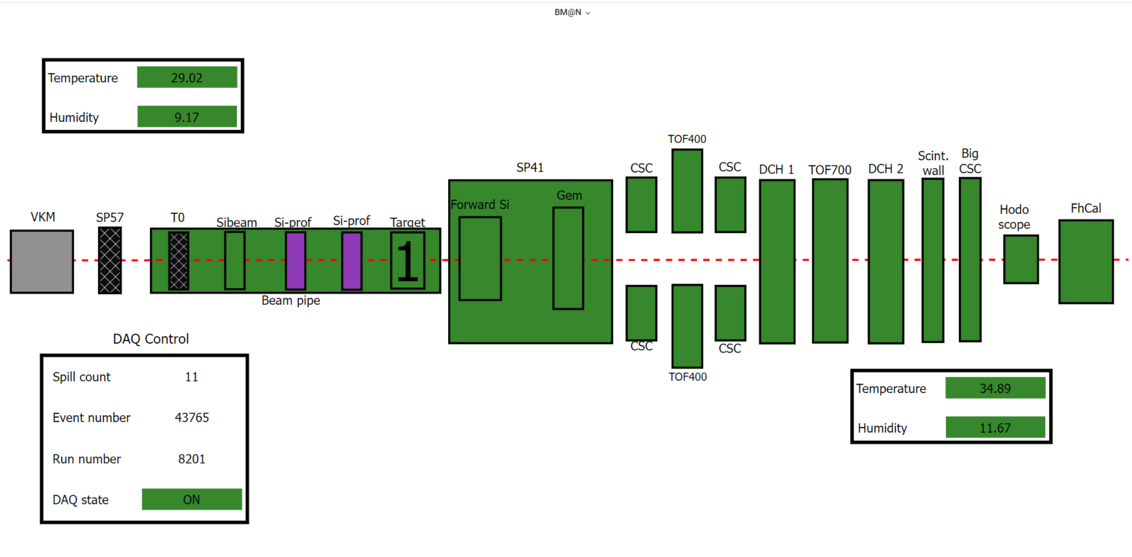

Figure 53: Slow Control System Main View.

TANGO Database, hosting the configuration of the whole system, and TANGO Historical Database are running on the BM@N virtual machine cluster. While programs, controlling and/or monitoring real hardware are running either on virtual cluster or on dedicated PCs of different subdetectors.

14 Summary

The detailed description of BM@N spectrometer is given. In this configuration t the fall of 2022 and the beginning of 2023 a big data set was recorded during 3 moths period. About 500M events with the different trigger condition are available for a physical analysis. A preliminary ananlysis of about 1% of data shows a signals particles decays with strange quarks (K^0_S, Λ). The signature of charge pions, kaons and protons is visible if the time flight system TOF400/TOF700 is involved in the data analysis. The resolution in particle momentum, the width of the invariant mass distributions are in agreement with the expected values estimated by MC simulation. The BM@N collaboration acknowledges the efforts of the staff of the accelerator division of the Laboratory of High Energy Physics at JINR that made the data taking possible and successful. The BM@N collaboration acknowledges support .....

References

[1] M. Kapishin (for the BM@N Collaboration), Eur. Phys. J. A52 (2016) no. 8, 213.

[2] J. Randrup and J. Cleymans, Phys. Rev. C 74 (2006) 047901.

[3] B. Friman, W. Nörenberg, and V.D. Toneev, Eur. Phys. J. A 3 (1998).

[4] NICA White Paper, Eur. Phys. J. A 52 (2016).

[5] BM@N Conceptual Design Report: http://nica.jinr.ru/files/BM@N/BMN_CDR.pdf

[6] Ch. Fuchs, Prog. Part. Nucl. Phys. 56 (2006) 1-103.

[7] P. G. Akishin *et al.* Optimization of a Large Aperture Dipole Magnet for Baryonic Matter Studies at Nuclotron, Phys. Part. Nucl. Lett. 2015. V. 12. P. 305

[8] A. Ivashkin *et al.* http://mpd.jinr.ru/doc/mpd-tdr/ 2017

[9] F. Guber *et al.* http://repository.gsi.de/record/109059/files/20150720 2015

[10] A. Izvestnyy, N. Karpushkin, F. Guber, S. Morozov and O. Petukhov, Calibration of FHCal with cosmic muons at the BM@N experiment, J. Phys. Conf. Ser. 1690 (2020) no.1, 012060.

[11] N. Karpushkin *et al.* Study of the hadron calorimeters response for CBM and BM@N experiments at hadron beams, J. Phys. Conf. Ser., 2020. 2̆0132̆013 Vol. 1667, no. 1. P012020. DOI: 10.1088/17426596/1667/1/012020.

[12] O. Petukhov, S. Morozov, Development of Detector Control System (DCS) for forward hadron calorimeters in the BM@N and the MPD experiments, J.Phys.Conf.Ser. 1690 (2020) 1, 012063, DOI: 10.1088/1742-6596/1690/1/012063

[13] D. Baranov *et al.* GEM tracking system of the BM@N experiment, 2017 JINST 12 C06041. DOI 10.1088/1748-0221/12/06/C06041.

[14] A. Galavanov *et al.* Status of the GEM/CSC tracking system of the BM@N experiment, 2020 JINST 15 C09038. DOI 10.1088/1748-0221/15/09/C09038.

[15] A. Galavanov *et al.* Performance of the BM@N GEM/CSC tracking system at the Nuclotron beam, 2019 EPJ Web Conf. 204 07009, https://doi.org/10.1051/epjconf/201920407009 .

[16] D. Bederede *et al.* Nucl. Instr. and Meth. A 367 (1995) 88.

[17] I. Augustin *et al.* Nucl. Instr. and Meth. A 403 (1998) 472.

[18] RedHat. Optimizing RHEL 9 for Real Time for low latency operation.
(*https : //access.redhat.com/documentation/en − us/red*$_h$*at*$_e$*nterprise*$_l$*inux*$_f$*or*$_r$*eal*$_t$*ime*/9)

[19] S. Weil et al. Ceph: A Scalable, High-Performance Distributed File System. OSDI 2̆01906: 7th USENIX Symposium on Operating Systems Design and Implementation.
(*https : //ceph.com/assets/pdfs/weil − ceph − osdi06.pdf*)

[20] Tango is an Open Source solution for SCADA and DCS.
(*https : //www.tango − controls.org/*)

[21] PostgreSQL is a powerful, open source object-relational database.
(*https : //www.postgresql.org/*)

[22] Grafana is a multi-platform open source analytics and interactive visualization web application.
(*https : //grafana.com/*)